3×10^4 cells/well in a 24-well culture dish and were transfected with 40 ng of NF-κB reporter plasmid (pNF-κB-Luc; BD Biosciences/BD Clontech), 2 ng of *NEMO* mutant expression construct, 10 ng of internal control for the normalization of transfection efficiency (pRL-TK; Toyo Ink), and 148 ng of mock vector using FuGENE HD Transfection Reagent (TOYO-B-Net) according to the manufacturer's protocol. Twelve hours after transfection, the cells were stimulated with 15 ng/mL lipopolysaccharide (LPS; Sigma-Aldrich) for 4 hours and the NF-κB activity was measured using the PicaGene Dual SeaPansy assay kit (TOYO-B-Net). Experiments were performed in triplicate and firefly luciferase activity was normalized to *Renilla* luciferase activity.

Subcloning analysis of cDNA

Cell sorting of the various cell lineages was performed by FACSVantage (BD Biosciences). The purity of each lineage was > 95%. The cDNA from sorted cells was purified and reverse transcribed by Super Script III (Invitrogen) with random hexamers and amplified by the proofreading PCR enzyme KOD, as previously described.[17,21] The PCR primers used were NEMO2 (5′-AGAGACGAAGGAGCACAAAGCTGCCTTGAG-3′) and NEMO3 (5′-ACTGCAGGGACAATGGTGGGTGCATCTGTC-3′). The PCR products were subcloned using a TA cloning kit (Invitrogen) and sequenced by ABI 3130xl Genetic analyzer (Applied Biosystems). To determine whether additional mutations occurred in revertant subclones that had wild-type sequence in the original mutation site, the entire coding region of the *NEMO* gene was sequenced and an additional mutation was considered present when the same mutation was detected in multiple subclones.

Allele-specific PCR

The mRNA purified from sorted T cells and monocytes was reverse-transcribed by SuperScript III (Invitrogen) with the gene-specific primer NEMO2 and amplified by the proofreading PCR enzyme KOD (Toyobo) using the primers NEMO3 and NEMO 4 (5′-TGTGGACACGCAGTGAAACGTGGTCTGGAG-3′). The PCR products were used as templates for allele-specific PCRs with Ex Taq polymerase (Takara Bio). Mutant and wild-type *NEMO* DNA was generated from each NEMO expression plasmid, mixed at graded ratios, and used as controls. PCR conditions and primer sequences are listed in supplemental Table 1 (available on the *Blood* Web site; see the Supplemental Materials link at the top of the online article).

Proliferation of NEMO^{normal} and NEMO^{low} T cells

To obtain PHA-induced T-cell blasts, PBMCs were stimulated with PHA (1:100; Invitrogen) and cultured in RPMI 1640 supplemented with 5% FCS and recombinant human IL-2 (50 IU/mL; kindly provided by Takeda Pharmaceutical Company) at 37°C for 7 days. Subcloning analysis of the cDNA obtained from the T-cell blasts was performed as described in "Subcloning analysis of cDNA."

Results

Reversion mosaicism of NEMO occurred in siblings with similar immunologic phenotypes

We previously reported patient 1 with a duplication mutation of the *NEMO* gene spanning intron 3 to exon 6, who was diagnosed as XL-EDA-ID at 1 year of age after suffering from recurrent infections.[17] At first, genetic diagnosis of the patient was difficult because the expression of aberrant *NEMO* mRNA was masked by the expression of normal *NEMO* mRNA by the revertant cells. Flow cytometric analysis of intracellular NEMO expression revealed cells with normal (NEMO^{normal}) and reduced (NEMO^{low}) levels of NEMO expression, indicating the presence of reversion mosaicism of the *NEMO* gene, and further analysis revealed that the *NEMO* mutation was disease-causing. PCR across the mutated region and sequencing of the PCR products revealed a duplication extending from intron 3 to exon 6, which was confirmed by Southern blot analysis. Additional copy number analysis of the *NEMO* gene of patient 1 and his mother excluded the possibility of a complex chromosomal aberration such as multiple duplication of the *NEMO* gene (supplemental Figure 1). Furthermore, polymorphism analysis using variable number tandem repeats on NEMO^{normal} and NEMO^{low} cells from patient 1 revealed that these cells were derived from the same origin (supplemental Table 2), indicating that the *NEMO* gene mosaicism was less likely because of amalgamation. The genomic analysis of the NEMO^{normal} cells revealed a complete reversion of the *NEMO* gene with no additional mutations. The clinical phenotype of patient 1 was combined immunodeficiency with a reduced number of T cells and mitogen-induced proliferation (Tables 2-3). We previously determined that reduced NEMO expression in the mutant T cells caused impairment of T-cell development and mitogen-induced proliferation.

Patient 2, the younger brother of patient 1, was diagnosed as XL-EDA-ID with the same duplication mutation as his brother. Flow cytometric analysis of intracellular NEMO expression performed at diagnosis showed that most of his PBMCs had reduced NEMO expression (Figure 1A). At 2 months of age, when most of the T cells were NEMO^{low}, absolute counts of the patient's T cells and the mitogen-induced proliferation of the patient's PBMCs were comparable with those of the healthy controls (Figure 1A-B; Table 2). These findings indicated that the *NEMO* mutation had no effect on T-cell development and mitogen-induced proliferation during early infancy in patient 2.

NEMO^{normal} T cells gradually increased as patient 2 grew older, while the absolute count of NEMO^{low} T cells decreased (Figure 1A-B). Accordingly, normal full-length *NEMO* cDNA, which had been undetectable in cord blood, was detectable in the patient's peripheral blood at 12 months of age. However, while NEMO^{normal} T cells were increasing, mitogen-induced T-cell proliferation started to decrease (Table 3), and the patient started to show poor weight gain from 6 months of age. When patient 2 was 17 months old, a blood culture revealed an *M szulgai* bacteremia. At this time, the absolute count of NEMO^{normal} T cells peaked, and NEMO^{low} T cells were at a minimum. He began to gain weight after anti-*Mycobacterium* medication was initiated, although NEMO^{normal} T cells started to decrease and NEMO^{low} T cells began to increase (Figure 1B). When the patient was 23 months old, mitogen-induced T-cell proliferation was still low and a roughly equal number of NEMO^{low} and NEMO^{normal} T cells were detected (Table 3). Overall, as patient 2 grew older, NEMO^{normal} T cells increased as the total number of T cells and the mitogen-induced T-cell proliferation decreased, similar to what had occurred in patient 1 at a similar age.

Various analyses were performed to compare the immunologic phenotype of NEMO^{low} and NEMO^{normal} T cells in detail. Both NEMO^{normal} and NEMO^{low} CD4$^+$ T cells carried a diverse Vβ repertoire, but CD8$^+$ T cells had a skewed Vβ repertoire regardless of NEMO expression level (Figure 1C). Surface marker analysis revealed that most of the NEMO^{normal} T cells were CD45RA$^-$/CCR7$^-$ and most of the NEMO^{low} T cells were CD45RA$^+$/CCR7$^+$ (Figure 1D). The NEMO^{normal} T cells produced similar amounts of IFN-γ and TNF-α as healthy control cells, while the production of these cytokines were reduced in NEMO^{low} T cells (Figure 1E-F). Taken together, these data implied that the immunologic phenotype of T cells from patient 2 converged with that of patient 1 as patient 2 grew older.

Table 2. Surface marker analysis of peripheral mononuclear cells of patients 1 and 2

	Patient 1	Patient 2		Healthy controls
Age at analysis	2 y	2 mo	19 mo	
CD3	1503	2366	1014	2997 ± 1751
CD4	292	1583	374	1683 ± 874
CD8	1160	783	547	1114 ± 976
TCRαβ	1386	2295	439	2620 ± 1612
TCRγδ	109	74	574	343 ± 177
$CD4^+CD45RA$	58	1336	105	1471 ± 890
$CD4^+CD45RO$	263	307	266	497 ± 189
$CD8^+CD45RA$	1178	783	297	1083 ± 1078
$CD8^+CD45RO$	361	21	250	385 ± 442
$CD4^+CD25$	80	427	93	210 ± 99
CD19	1200	941	1543	1252 ± 1145
CD20	1189	931	1536	1125 ± 837
$CD19^+$Sm-IgG	7	18	17	54 ± 21
$CD19^+$Sm-IgA	15	4	14	18 ± 14
$CD19^+$Sm-IgM	1171	910	1505	1057 ± 881
$CD19^+$Sm-IgD	1171	906	1495	1052 ± 884
CD16	912	176	24	287 ± 200
CD56	908	176	24	306 ± 207

Surface markers expressed by XL-EDA-ID patients' PBMCs are shown as absolute counts per microliter of peripheral blood. Healthy control values are based on children aged 1 to 6 years and are shown as the mean ± SD.

Sm indicates the surface membrane.

High incidence of somatic mosaicism of the *NEMO* gene in XL-EDA-ID patients

It is worth noting that somatic reversion mosaicism of the *NEMO* gene occurred in both of the 2 XL-EDA-ID siblings carrying a duplication mutation. To determine whether a high frequency of reversion is a specific event for this type of *NEMO* duplication mutation[22-25] or if the reversion of the *NEMO* gene occurs commonly in XL-EDA-ID patients, we recruited an additional 8 XL-EDA-ID patients from throughout Japan (Table 1) and analyzed the presence of *NEMO* reversion. These patients had various combinations of clinical phenotypes characteristic of XL-EDA-ID such as ectodermal dysplasia, innate and acquired immunity defects, and susceptibility to pyogenic bacteria and *Mycobacterium* infections. Every patient had a mutation of the *NEMO* gene with reduced NF-κB activation potential, as evaluated in a NEMO reconstitution assay (Figure 2).

Among the 8 patients, only patient 3 had a large proportion of $NEMO^{low}$ cells by flow cytometric analysis. The majority of patient 3's PBMCs were $NEMO^{low}$, whereas 10% of the patient's $CD8^+$ cells were $NEMO^{normal}$ (Figure 3A). This patient was identified as carrying the D311E mutation. Because missense mutations of the *NEMO* gene often do not result in the reduced expression of NEMO protein, subcloning and sequencing analysis was performed on the *NEMO* cDNA isolated from the remaining patients, and 6 of the 7 patients had normal *NEMO* subclones (Table 3). Expansion of maternal cells after fetomaternal transfusion was ruled out in these patients by FISH analysis with X and Y probes (Table 1).

Additional genetic analysis of the entire coding region of the *NEMO* gene was performed on $NEMO^{normal}$ cells from patient 3 and on reverted subclones from the other patients, except for patient 10 who had already received stem cell transplantation. The *NEMO* gene in these samples had reverted to wild-type with no additional mutations (Figure 3B and data not shown). To specifically determine in which cell lineages the reversion occurred, subcloning and sequencing analysis of cDNA in various cell lineages was performed. This analysis revealed that all the revertant cells were of the T-cell lineage and that no reversion occurred in monocytes and very little occurred in B cells (Table 4). Allele-specific PCR confirmed that reversion occurred in T cells but not in monocytes (Figure 4).

Selective advantage of $NEMO^{normal}$ cells in XL-EDA-ID carriers

The high frequency of somatic mosaicism in T cells of XL-EDA-ID patients indicated a strong selective advantage of wild-type NEMO T cells over T cells carrying mutant NEMO. To confirm this hypothesis, *NEMO* cDNA analysis was performed on various cell lineages from the mothers of the patients who are heterozygous for *NEMO* mutation and thus have mosaicism

Table 3. Immunologic analysis of patients 1 and 2

	Patient 1	Patient 2 (treated with IVIG)	
Age at analysis, mo	9	9	20
Serum immunoglobulin levels, g/L (control)			
IgG	10.63 (4.51-10.46)	8.44 (4.51-10.46)	10.37 (7.15-9.07)
IgA	1.36 (0.14-0.64)	1.88 (0.14-0.64)	3.93 (0.22-1.44)
IgM	0.4 (0.33-1.00)	0.17 (0.33-1.00)	0.20 (0.34-1.28)
Age at analysis	2 y	2 mo	23 mo
T-cell proliferation, SI (control)	9.3 (206.9 ± 142.5)	55.3 (64.8 ± 8.1)	7.2 (89.4 ± 31.2)

Control values of serum immunoglobulin levels are based on children aged either 7 to 9 months or 1 to 2 years and are shown as the mean ± SD. The T-cell proliferation assay was performed as described previously[17] with at least three healthy adults as controls.

SI indicates stimulation index; and IVIG, 2.5 g of monthly IV immune globulin infusion.

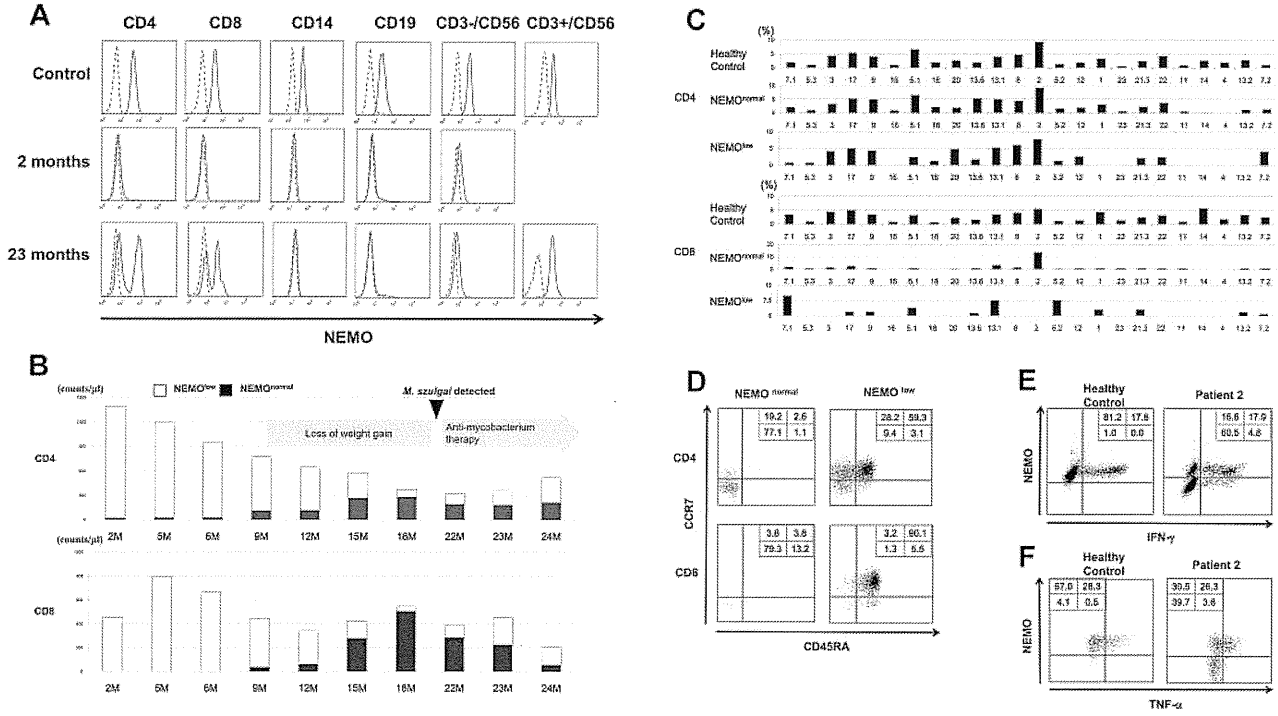

Figure 1. Identification and characterization of *NEMO* revertant T cells in patient 2. (A) Intracellular expression of NEMO in various PBMC lineages from a healthy adult control and patient 2 were evaluated by flow cytometry. For the patient, results of the analyses performed at 2 months and 23 months are shown. Solid lines indicate staining with the anti-NEMO mAb, and dotted lines indicate the isotype control. (B) Time-course variations in the absolute count of $NEMO^{normal}$ and $NEMO^{low}$ T cells in patient 2. M indicates age in months. (C) TCR-Vβ repertoire analysis of the patient's $CD4^+$ and $CD8^+$ T cells. PBMCs from the patient and a healthy adult control were stained for the TCR-Vβ panel, CD4, CD8, and NEMO, and analyzed by flow cytometry. (D) Phenotype analysis of T cells in patient 2. PBMCs from the patient and a control were stained for the expression of NEMO, CCR7, CD45RA, and CD4 or CD8. Data shown were gated on $NEMO^{normal}$ or $NEMO^{low}$ $CD4^+$ or $CD8^+$ cells. (E-F) Cytokine production from $NEMO^{normal}$ and $NEMO^{low}$ T cells. PBMCs from the patient and a control were stimulated with PMA and ionomycin for 6 hours and stained for intracellular (E) IFN-γ or (F) TNF-α along with NEMO. Cells shown are gated on the $CD3^+$ population.

because of X-chromosome inactivation. This analysis assumes that the percentage of cDNA for wild-type *NEMO* reflects the percentage of cells expressing wild-type NEMO. A high proportion of wild-type *NEMO* cDNA was observed in T cells from the mothers of patients 1/2, 3, 8, and 10, although wild-type *NEMO* cDNA was not predominant in T cells from the mother of patient 4 (Table 5).

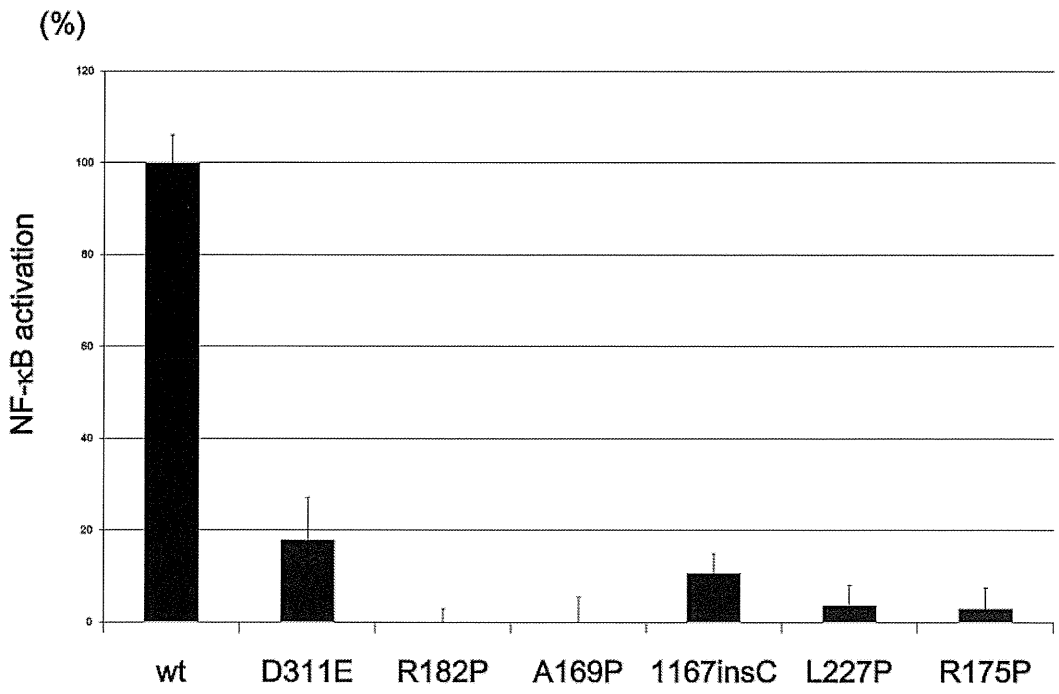

Figure 2. NF-κB transactivation by NEMO mutants from the XL-EDA-ID patients. NF-κB transactivation induced by NEMO mutants in the XL-EDA-ID patients. Mock vectors and wild-type (wt) NEMO were used as controls. The NF-κB activation index of NEMO variants were calculated as (NF-κB activation by each NEMO variant − NF-κB activation of the mock vector)/(NF-κB activation by wild-type NEMO − NF-κB activation of the mock vector). The data shown are the mean ± SD of triplicate wells and are representative of 3 independent experiments with similar results.

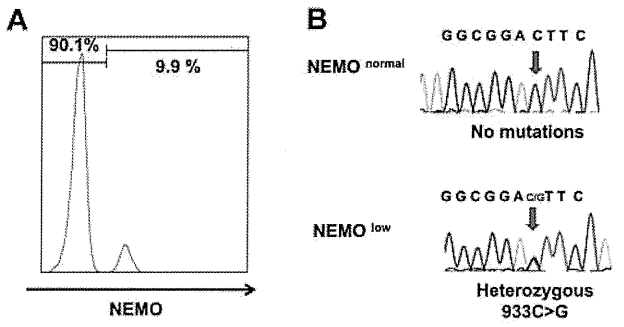

Figure 3. *NEMO* revertant T cells in patient 3. (A) Intracellular expression of NEMO in CD8$^+$ cells from patient 3. (B) Sequencing chromatograms of DNA from NEMO^{normal} or NEMO^{low} CD8$^+$ cells of patient 3. Arrows indicate the mutated base position at c. 931.

Similarly, there was an apparent high proportion of wild-type *NEMO* cDNA in monocytes and B cells from the mothers of patients 1/2, 8, and 10 (Table 5). These findings suggested a general selective advantage of NEMO^{normal} cells over NEMO^{low} cells in vivo, especially in T cells.

Proliferation capacity of NEMO^{normal} and NEMO^{low} T cells

T-cell proliferation stimulated by mitogens such as PHA is usually not reduced in XL-EDA-ID patients. However, the emergence of NEMO^{normal} cells coincided with a reduction in mitogen-induced proliferation in patient 2. To further determine the effect of NEMO^{normal} cells on mitogen-induced proliferation of peripheral T cells, the proportions of T cells carrying the wild-type and mutant were examined before and after PHA stimulation in XL-EDA-ID patients and their mothers (Table 6). In patients 2, 4, and 8, the percentage of the NEMO^{normal} cells decreased after PHA stimulation, while NEMO^{normal} cells prevailed in patient 9. In the mothers of patient 4 and 10, the percentage of NEMO^{normal} cells increased after PHA stimulation, while the percentage of the NEMO^{normal} cells decreased in the mother of patient 3. These results indicated that the NEMO mutation does not directly affect the mitogen-induced proliferation capacity of T cells and factors other than the *NEMO* genotype determine the proliferation capacity of NEMO^{normal} and NEMO^{low} T cells.

Discussion

Somatic reversion mosaicism has been described in several disorders affecting the hematopoietic system, the liver, and the skin.[23,26] Reports of somatic reversion cases have been particularly abundant in patients with immunodeficiency diseases, including Wiskott-Aldrich syndrome (WAS)[27] and SCID, which occur because of mutations in the interleukin receptor common γ chain,[28] CD3ζ,[29] *RAG-1*[30], and *ADA* genes.[31] Patients with somatic reversion mosaicism may present with significantly milder clinical phenotypes compared with nonrevertant patients with the same germline mutation, although this is not always the case.[26] One common feature in most cases where the somatic reversion mosaicism has been observed is a strong in vivo selective advantage of the revertant cells that express the wild-type gene product. One of the most intensively investigated diseases associated with somatic reversion mosaicism is WAS.[32-34] A report showed that up to 11% of WAS patients have presented with somatic reversion mosaicism.[33]

In our investigation, 9 of 10 XL-EDA-ID patients presented with somatic mosaicism. Two of the 9 were cases of reversion from a duplication mutation, while the others exhibited true back-reversion from a substitution or insertion mutation. This finding calls for caution when diagnosing XL-EDA-ID patients. Because the existence of a *NEMO* pseudogene makes it difficult to perform genetic analysis using genomic DNA, diagnosis of the disease is often confirmed by sequencing analysis of *NEMO* cDNA, and the presence of somatic mosaicism can cause misdiagnosis of XL-EDA-ID patients either when NEMO^{normal} cells make up the majority of the patients' PBMCs or when the cDNA of the mutated *NEMO* gene cannot be amplified by PCR.[17] In fact, mutated *NEMO* cDNA could not be amplified from the PBMCs of patient 2 even when NEMO^{normal} cells were absent (during early infancy), and only wild-type *NEMO* cDNA was amplified after the appearance of NEMO^{normal} cells (data not shown), probably because of the instability of the mutated *NEMO* mRNA. Flow cytometric analysis of intracellular NEMO protein is of help in identifying the NEMO^{low} cells in some patients, but the technique is not applicable when the *NEMO* mutation does not cause reduced expression of NEMO protein. Thus, some cases of XL-EDA-ID patients with reversion may be difficult to diagnose.

The high frequency of somatic mosaicism observed in XL-EDA-ID patients indicates a strong in vivo selective advantage for NEMO^{normal} cells, which express the wild-type gene product. Patient 2 presented with a high mutant T-cell count at birth that gradually decreased over time (Figure 1B). This finding indicates that wild-type NEMO expression is critical for the survival of certain cell lineages, including T cells, after birth. On the other hand, no NEMO^{normal} monocytes and very few NEMO^{normal} B cells were detected in the recruited XL-EDA-ID patients (Table 4). This specific feature is similar to other somatic reversion mosaicism seen in primary immunodeficiency patients[26] and indicates that the expression of NEMO is less critical for the survival of monocytes or B cells compared with that of T cells. There is also an apparent

Table 4. Analysis of *NEMO* gene mosaicism in various cell lineages for each patient

Patient	Mutation	Age at analysis	CD4, % (proportion)	CD8, % (proportion)	CD14, % (proportion)	CD19, % (proportion)
1	Duplication	2 y	90	100	0	4.0
2	Duplication	15 mo	45	66	0	4.0
3	D311E	3 y	2.4	9.9	0	1.2
4	A169P	12 y	0 (0/19)	24 (9/37)	0 (0/19)	0 (0/47)
5	L227P	3 y	0 (0/25)	0 (0/35)	0 (0/30)	0 (0/25)
6	R182P	4 y	18 (5/28)	17 (9/52)	0 (0/27)	0 (0/33)
7	R175P	6 y	0.4 (1/25)	39 (11/28)	0 (0/28)	0 (0/25)
8	Q348X	8 y	38 (6/16)	47 (9/19)	0 (0/33)	0 (0/25)
9	R175P	15 y	30 (9/30)	36 (12/33)	0 (0/23)	0 (0/14)
10	1167 ins C	9 mo		PBMC 9.3 (4/43)		

For patients 1 to 3, data represent the percentages of NEMO^{normal} cells in each lineage, as assessed by flow cytometry. For patients 4 to 10, the ratio indicates the number of wild-type NEMO clones in various cell lineages as compared with the total number of clones analyzed, based on subcloning and sequencing analysis.

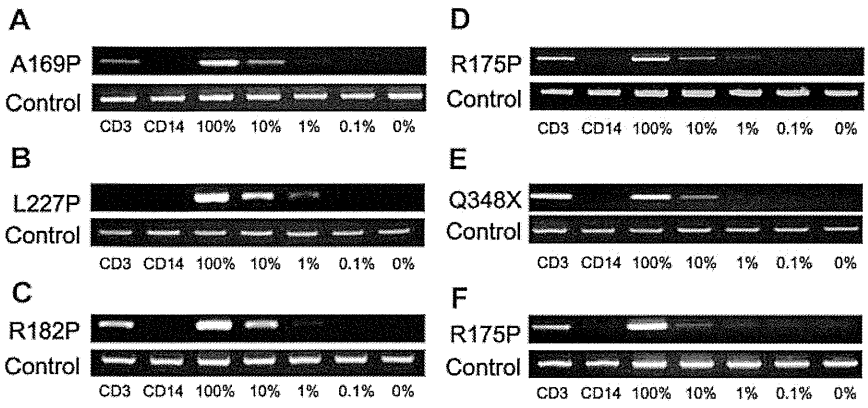

Figure 4. NEMO reversion selectively occurs in T cells of XL-EDA-ID patients. Allele-specific PCR for *NEMO* on $CD3^+$ or $CD14^+$ cells from (A) patient 4, (B) patient 5, (C) patient 6, (D) patient 7, (E) patient 8, and (F) patient 9. Numbers below each figure indicate the percentages of wild-type NEMO cDNA mixed with each mutant. Primers used in each PCR are shown on the left.

concordance between the degree of the disruption of *NEMO* gene and the proportion of reverted $NEMO^{normal}$ cells compared with $NEMO^{low}$ cells. The high proportion of reverted T cells seen in patients 1 and 2 as well as in patient 8 was associated with a highly disruptive mutation of the *NEMO* gene (ie, a duplication mutation in patients 1 and 2, and a truncation mutation in patient 8). In addition, the highly selective X-chromosome inactivation observed in the mothers of XL-EDA-ID patients indicated a strong selective advantage for $NEMO^{normal}$ cells over $NEMO^{low}$ cells. It is also noteworthy that reverted T cells were not detected in patient 5, who carried an L227P mutation that was not localized to either of the functional domains in the NEMO protein. Other reported cases with the same mutation presented with polysaccharide-specific humoral immunodeficiency and autoinflammatory diseases, but were spared complications such as cellular immunodeficiency and susceptibility to *Mycobacterium* (similar to patient 5).[4,8] This may reflect the fact that the L227P mutation in NEMO has less influence on T-cell growth than NEMO mutations that occur in functional domains, and suggests that reversion of the mutation has little impact on T-cell survival. Although the number of cases in our study is limited, it appears that the more disruptive NEMO mutations favor the survival of $NEMO^{normal}$ cells after reversion and X-chromosome inactivation.

Regarding the gradual decline in the number of NEMO-deficient T cells, one candidate trigger could be infection. Because the dominance of the memory phenotype and the skewed TCR repertoire among $CD8^+$ T cells in $NEMO^{normal}$ cells were observed in both patients 1 and 2 (Figure 1C and Mizukami et al[18]), continuous infection of pyogenic bacteria in patient 1 and *M szulgai* in patient 2 could be a reason for the emergence of $NEMO^{normal}$ cells and the elimination of $NEMO^{low}$ cells. The decrease in $NEMO^{normal}$ cells and restoration of $NEMO^{low}$ cells after anti-mycobacterial therapy in patient 2 support this hypothesis. In the case of patient 1, the predominance of $NEMO^{normal}$ T cells with an effector/memory phenotype at diagnosis (Table 4 and Mizukami et al[18]) is likely to be the result of chronic infection, and it is possible that $NEMO^{low}$ cells were predominant during his early infancy. Because some reports have indicated that TNF-α–induced programmed cell death of several cell types, including a human T-cell line, was enhanced by hypomorphic *NEMO* mutations,[12,35] and considering our finding that the levels of TNF-α expressed in revertant T cells were similar to levels in healthy control T cells in vitro (Figure 1F), TNF-α produced from these cells in response to infection could be involved in mutant T-cell elimination.

Unexpectedly, T-cell proliferation in patient 2 was equivalent to that of normal controls at the age of 2 months and was reduced after $NEMO^{normal}$ T cells increased (Figure 1B; Table 3). This finding indicates that the $NEMO^{low}$ T cells did not have intrinsically impaired mitogen-induced proliferation. One reasonable explanation for the reduced proliferation observed after the increase in $NEMO^{normal}$ T cells is a reduction in the absolute number of T cells (naive T cells in particular), probably because of the infection.

Table 5. Expression of mutant NEMO in various cell lineages for the mother of each XL-EDA-ID patient

Sample	Mutation	Analysis	Subtype	Mutant type, % (proportion)
Mother of patients 1 and 2	Duplication	FACS	CD3	0
			CD14	0
			CD19	0
Mother of patient 3	D311E	FACS	CD3	13
			$CD3^-$	54
		Subcloning	CD3	22 (6/27)
			$CD3^-$	55 (12/22)
Mother of patient 4	A169P	Subcloning	CD3	52 (11/21)
			CD14	58 (11/19)
			CD19	42 (5/12)
Mother of patient 8	Q348X	Subcloning	CD3	0 (0/26)
			CD14	17 (3/18)
			CD19	0 (0/18)
Mother of patient 10	1167insC	Subcloning	CD3	18 (7/39)
			CD14	12 (5/43)
			CD19	27 (12/44)

Data are shown as either the percentages of $NEMO^{normal}$ cells, as assessed by flow cytometry, or as the ratio of clones containing wild-type NEMO to the total number of clones, as analyzed by subcloning and sequencing analysis.

Table 6. Expression of mutant NEMO in CD3-positive cells and PHA blasts

Sample	Mutations	Analysis	Subtype	Mutant type, % (proportion)
Mother of patient 3	D311E	FACS	CD3	13
			PHA blast	47
		Subcloning	CD3	22 (6/27)
			PHA blast	48 (11/23)
Mother of patient 4	A169P	Subcloning	CD3	52 (11/21)
			PHA blast	18 (9/49)
Mother of patient 8	Q348X	Subcloning	CD3	0 (0/26)
			PHA blast	0 (0/21)
Mother of patient 10	1167insC	Subcloning	CD3	18 (7/39)
			PHA blast	9 (4/43)
Patient 2	Duplication	FACS	CD3	73
			PHA blast	93
Patient 4	A169P	Subcloning	CD3	79 (19/24)
			PHA blast	100 (37/37)
Patient 8	Q348X	Subcloning	CD3	56 (18/32)
			PHA blast	100 (16/16)
Patient 9	R175P	Subcloning	CD3	87 (34/39)
			PHA blast	0 (0/28)

PHA blasts were obtained by incubating PBMCs with PHA and soluble IL-2 for 7 days. Data are shown as either the percentages of $NEMO^{normal}$ cells, as assessed by flow cytometry, or as the ratio of clones containing wild-type NEMO to the total number of clones, as analyzed by subcloning and sequencing analysis.

Therefore, to identify other mechanisms underlying reduced T-cell proliferation, the impact of *NEMO* mutation on PHA-induced T-cell proliferation was indirectly examined in vitro by comparing the response of $NEMO^{normal}$ and $NEMO^{low}$ cells derived from XL-EDA-ID patients and their mothers. After PHA stimulation and proliferation, the proportion of $NEMO^{low}$ T cells increased in patients 2, 4, and 8, while the opposite result was observed in patient 9 and in the mother of patient 4 (Table 6). Although the precise mechanism is unclear, a reduction in the proportion of $NEMO^{normal}$ cells after PHA stimulation would reflect the lower proliferative capacity of $NEMO^{normal}$ cells compared with that of $NEMO^{low}$ cells, which may be another explanation for the reduced T-cell proliferation observed in patient 2 at 23 months of age when $NEMO^{normal}$ T cells were dominant. In the reports on reversion mosaicism of *IL2RG* gene mutations,[28,36] the restoration of T-cell function and clinical symptoms varied among patients. Therefore, other factors besides the genotype of the mutations, such as the developmental stage where reversion occurred and the frequency of reversion, affect the clinical impact of somatic mosaicism of *NEMO* gene mutations.

In this study, the effect of somatic mosaicism of the *NEMO* gene on clinical phenotype could not be fully evaluated. However, cytokines produced by revertant T cells could influence the development of clinical symptoms of XL-EDA-ID, such as inflammatory bowel disease. In a mouse model, intestinal epithelial cell-specific inhibition of NF-κB through the conditional ablation of NEMO resulted in the development of chronic bowel inflammation sensitized intestinal epithelial cells to TNF-α–induced apoptosis.[37] In this model, the first phase of intestinal inflammation was initiated by epithelial cell death and was followed by a second phase of TNF-α–induced intestinal inflammation, the latter being dependent on T cells. Another report showed that HSCT in XL-EDA-ID patients exacerbated the patients' inflammatory bowel disease.[38] Indeed, in patient 4, the percentage of reverted T cells was reduced after repeated administrations of anti-TNFα blocking Ab, and the symptoms of inflammatory bowel disease improved.[18] Considering this evidence, somatic mosaicism in T cells might be an important factor leading to inflammatory disease in XL-EDA-ID patients with defective NF-κB activation. However, our study did not show a tight association between inflammatory bowel disease and somatic mosaicism, and further investigation is needed to determine whether the $NEMO^{normal}$ T cells play a role in inflammatory processes in XL-EDA-ID.

In conclusion, this study has identified a high frequency of somatic mosaicism in XL-EDA-ID patients, particularly in T cells, and has revealed important insights into human T-cell immunobiology in XL-EDA-ID. Although we could not demonstrate the clinical impact of somatic mosaicism in XL-EDA-ID patients, our findings suggest that care is required when making molecular diagnoses of XL-EDA-ID, and might shed light on the mechanisms underlying the variability in the clinical manifestation of XL-ED-ID and facilitate the search for appropriate treatments.

Acknowledgments

The authors are grateful to all the XL-EDA-ID patients and their families for their participation. They also thank Shoji Yamaoka (Department of Molecular Virology, Graduate School of Medicine, Tokyo Medical and Dental University, Tokyo, Japan) for kindly providing NEMO-null rat fibroblast cells, and Takeda Pharmaceutical Company Limited for kindly providing the recombinant human IL-2.

This work was supported by grants from the Japanese Ministry of Education, Culture, Sports, Science, and Technology, and by grants from the Japanese Ministry of Health, Labor and Welfare.

Authorship

Contribution: Tomoki Kawai wrote the manuscript and performed research; R.N., T.Y., T.N., and T.H. edited the manuscript and supervised this work; K.I., Y.M., N.T., H.S., M.S., and Y.T. cultured cells; and T. Mizukami, H.N., Y.K., A.Y., T. Murata, S.S., E.I., H.A., Toshinao Kawai, C.I., S.O., and M.K. treated patients and analyzed data.

Conflict-of-interest disclosure: The authors declare no competing financial interests.

Correspondence: Ryuta Nishikomori, MD, PhD, Department of Pediatrics, Kyoto University Graduate School of Medicine, 54 Kawahara-cho, Shogoin, Sakyo-ku, Kyoto 606-8507, Japan; e-mail: rnishiko@kuhp.kyoto-u.ac.jp.

References

1. Pinheiro M, Freire-Maia N. Ectodermal dysplasias: a clinical classification and a causal review. *Am J Med Genet.* 1994;53(2):153-162.
2. Abinun M, Spickett G, Appleton AL, Flood T, Cant AJ. Anhidrotic ectodermal dysplasia associated with specific antibody deficiency. *Eur J Pediatr.* 1996;155(2):146-147.
3. Sitton JE, Reimund EL. Extramedullary hematopoiesis of the cranial dura and anhidrotic ectodermal dysplasia. *Neuropediatrics.* 1992;23(2):108-110.
4. Schweizer P, Kalhoff H, Horneff G, Wahn V, Diekmann L. [Polysaccharide specific humoral immunodeficiency in ectodermal dysplasia. Case report of a boy with two affected brothers]. *Klin Padiatr.* 1999;211(6):459-461.
5. Abinun M. Ectodermal dysplasia and immunodeficiency. *Arch Dis Child.* 1995;73(2):185.
6. Zonana J, Elder ME, Schneider LC, et al. A novel X-linked disorder of immune deficiency and hypohidrotic ectodermal dysplasia is allelic to incontinentia pigmenti and due to mutations in IKK-gamma (NEMO). *Am J Hum Genet.* 2000;67(6):1555-1562.
7. Courtois G, Smahi A, Israel A. NEMO/IKK gamma: linking NF-kappa B to human disease. *Trends Mol Med.* 2001;7(10):427-430.
8. Doffinger R, Smahi A, Bessia C, et al. X-linked anhidrotic ectodermal dysplasia with immunodeficiency is caused by impaired NF-kappaB signaling. *Nat Genet.* 2001;27(3):277-285.
9. Rothwarf DM, Zandi E, Natoli G, Karin M. IKK-gamma is an essential regulatory subunit of the IkappaB kinase complex. *Nature.* 1998;395(6699):297-300.
10. Yamaoka S, Courtois G, Bessia C, et al. Complementation cloning of NEMO, a component of the IkappaB kinase complex essential for NF-kappaB activation. *Cell.* 1998;93(7):1231-1240.
11. Smahi A, Courtois G, Vabres P, et al. Genomic rearrangement in NEMO impairs NF-kappaB activation and is a cause of incontinentia pigmenti. The International Incontinentia Pigmenti (IP) Consortium. *Nature.* 2000;405(6785):466-472.
12. Hanson EP, Monaco-Shawver L, Solt LA, et al. Hypomorphic nuclear factor-kappaB essential modulator mutation database and reconstitution system identifies phenotypic and immunologic diversity. *J Allergy Clin Immunol.* 2008;122(6):1169-1177.
13. Orange JS, Jain A, Ballas ZK, Schneider LC, Geha RS, Bonilla FA. The presentation and natural history of immunodeficiency caused by nuclear factor kappaB essential modulator mutation. *J Allergy Clin Immunol.* 2004;113(4):725-733.
14. Jain A, Ma CA, Liu S, Brown M, Cohen J, Strober W. Specific missense mutations in NEMO result in hyper-IgM syndrome with hypohydrotic ectodermal dysplasia. *Nat Immunol.* 2001;2(3):223-228.
15. Orange JS, Brodeur SR, Jain A, et al. Deficient natural killer cell cytotoxicity in patients with IKK-gamma/NEMO mutations. *J Clin Invest.* 2002;109(11):1501-1509.
16. Sebban H, Courtois G. NF-kappaB and inflammation in genetic disease. *Biochem Pharmacol.* 2006;72(9):1153-1160.
17. Nishikomori R, Akutagawa H, Maruyama K, et al. X-linked ectodermal dysplasia and immunodeficiency caused by reversion mosaicism of NEMO reveals a critical role for NEMO in human T-cell development and/or survival. *Blood.* 2004;103(12):4565-4572.
18. Mizukami T, Obara M, Nishikomori R, et al. Successful treatment with infliximab for inflammatory colitis in a patient with X-linked anhidrotic ectodermal dysplasia with immunodeficiency. *J Clin Immunol.* 2012;32(1):39-49.
19. Imamura M, Kawai T, Okada S, et al. Disseminated BCG infection mimicking metastatic nasopharyngeal carcinoma in an immunodeficient child with a novel hypomorphic NEMO mutation. *J Clin Immunol.* 2011;31(5):802-810.
20. Tono C, Takahashi Y, Terui K, et al. Correction of immunodeficiency associated with NEMO mutation by umbilical cord blood transplantation using a reduced-intensity conditioning regimen. *Bone Marrow Transplant.* 2007;39(12):801-804.
21. Saito M, Nishikomori R, Kambe N, et al. Disease-associated CIAS1 mutations induce monocyte death, revealing low-level mosaicism in mutation-negative cryopyrin-associated periodic syndrome patients. *Blood.* 2008;111(4):2132-2141.
22. Yang TP, Stout JT, Konecki DS, Patel PI, Alford RL, Caskey CT. Spontaneous reversion of novel Lesch-Nyhan mutation by HPRT gene rearrangement. *Somat Cell Mol Genet.* 1988;14(3):293-303.
23. Zhang LH, Jenssen D. Reversion of the hprt mutant clone SP5 by intrachromosomal recombination. *Carcinogenesis.* 1992;13(4):609-615.
24. Monnat RJ Jr, Chiaverotti TA, Hackmann AF, Maresh GA. Molecular structure and genetic stability of human hypoxanthine phosphoribosyltransferase (HPRT) gene duplications. *Genomics.* 1992;13(3):788-796.
25. Rautenstrauss B, Liehr T, Fuchs C, et al. Mosaicism for Charcot-Marie-Tooth disease type 1A: onset in childhood suggests somatic reversion in early developmental stages. *Int J Mol Med.* 1998;1(2):333-337.
26. Wada T, Candotti F. Somatic mosaicism in primary immune deficiencies. *Curr Opin Allergy Clin Immunol.* 2008;8(6):510-514.
27. Ariga T, Kondoh T, Yamaguchi K, et al. Spontaneous in vivo reversion of an inherited mutation in the Wiskott-Aldrich syndrome. *J Immunol.* 2001;166(8):5245-5249.
28. Stephan V, Wahn V, Le Deist F, et al. Atypical X-linked severe combined immunodeficiency due to possible spontaneous reversion of the genetic defect in T cells. *N Engl J Med.* 1996;335(21):1563-1567.
29. Rieux-Laucat F, Hivroz C, Lim A, et al. Inherited and somatic CD3zeta mutations in a patient with T-cell deficiency. *N Engl J Med.* 2006;354(18):1913-1921.
30. Wada T, Toma T, Okamoto H, et al. Oligoclonal expansion of T lymphocytes with multiple second-site mutations leads to Omenn syndrome in a patient with RAG1-deficient severe combined immunodeficiency. *Blood.* 2005;106(6):2099-2101.
31. Hirschhorn R. In vivo reversion to normal of inherited mutations in humans. *J Med Genet.* 2003;40(10):721-728.
32. Wada T, Schurman SH, Jagadeesh GJ, Garabedian EK, Nelson DL, Candotti F. Multiple patients with revertant mosaicism in a single Wiskott-Aldrich syndrome family. *Blood.* 2004;104(5):1270-1272.
33. Stewart DM, Candotti F, Nelson DL. The phenomenon of spontaneous genetic reversions in the Wiskott-Aldrich syndrome: a report of the workshop of the ESID Genetics Working Party at the XIIth Meeting of the European Society for Immunodeficiencies (ESID). Budapest, Hungary October 4-7, 2006. *J Clin Immunol.* 2007;27(6):634-639.
34. Davis BR, Yan Q, Bui JH, et al. Somatic mosaicism in the Wiskott-Aldrich syndrome: molecular and functional characterization of genotypic revertants. *Clin Immunol.* 2010;135(1):72-83.
35. Yamaoka S, Inoue H, Sakurai M, et al. Constitutive activation of NF-kappa B is essential for transformation of rat fibroblasts by the human T-cell leukemia virus type I Tax protein. *EMBO J.* 1996;15(4):873-887.
36. Speckmann C, Pannicke U, Wiech E, et al. Clinical and immunologic consequences of a somatic reversion in a patient with X-linked severe combined immunodeficiency. *Blood.* 2008;112(10):4090-4097.
37. Nenci A, Becker C, Wullaert A, et al. Epithelial NEMO links innate immunity to chronic intestinal inflammation. *Nature.* 2007;446(7135):557-561.
38. Fish JD, Duerst RE, Gelfand EW, Orange JS, Bunin N. Challenges in the use of allogeneic hematopoietic SCT for ectodermal dysplasia with immune deficiency. *Bone Marrow Transplant.* 2009;43(3):217-221.

Brief report

Identification of *TRIB1* R107L gain-of-function mutation in human acute megakaryocytic leukemia

Takashi Yokoyama,[1] Tsutomu Toki,[2] Yoshihiro Aoki,[2] Rika Kanezaki,[2] Myoung-ja Park,[3] Yohei Kanno,[1] Tomoko Takahara,[1] Yukari Yamazaki,[1] Etsuro Ito,[2] Yasuhide Hayashi,[3] and Takuro Nakamura[1]

[1]Division of Carcinogenesis, Cancer Institute, Japanese Foundation for Cancer Research, Tokyo, Japan; [2]Department of Pediatrics, Hirosaki University Graduate School of Medicine, Hirosaki, Japan; and [3]Department of Hematology/Oncology, Gunma Children's Medical Center, Gunma, Japan

Trib1 has been identified as a myeloid oncogene in a murine leukemia model. Here we identified a _TRIB1_ somatic mutation in a human case of Down syndrome–related acute megakaryocytic leukemia. The mutation was observed at well-conserved arginine 107 residue in the pseudokinase domain. This R107L mutation remained in leukocytes of the remission stage in which _GATA1_ mutation disappeared, suggesting the _TRIB1_ mutation is an earlier genetic event in leukemogenesis. The bone marrow transfer experiment showed that acute myeloid leukemia development was accelerated by transducing murine bone marrow cells with the R107L mutant in which enhancement of ERK phosphorylation and C/EBPα degradation by Trib1 expression was even greater than in those expressing wild-type. These results suggest that TRIB1 may be a novel important oncogene for Down syndrome–related acute megakaryocytic leukemia. (_Blood._ 2012; 119(11):2608-2611)

Introduction

The Down syndrome (DS) patients are predisposed to developing myeloid leukemia, and those patients frequently exhibit *GATA1* mutations.[1] However, it is proposed that the *GATA1* mutation is important for transient leukemia in DS but not sufficient for full-blown leukemia, suggesting that additional genetic alterations are needed.[1] Therefore, it is important to search the subsequent genetic changes for DS-related leukemia (ML-DS) to predict malignant transformation and prognosis of the patients.

Trib1 has been identified as a myeloid oncogene that cooperates with *Hoxa9* and *Meis1* in murine acute myeloid leukemia (AML).[2] As a member of the tribbles family of proteins, TRIB1 interacts with MEK1 and enhances ERK phosphorylation.[2,3] Moreover, TRIB1 promotes degradation of C/EBP family transcription factors, including C/EBPα, an important tumor suppressor for AML, and we observed that degradation of C/EBPα by Trib1 is mediated by its interaction with MEK1.[4] Thus, TRIB1 plays an important role in the development of AML by modulating both the RAS/MAPK pathway and C/EBPα function together with Trib2 that has also been identified as a myeloid-transforming gene.[5] Potential involvement of *TRIB1* in human leukemia has been reported in cases of AML with 8q34 amplification in which both *c-MYC* and *TRIB1* are included in the amplicon.[6] The enhancing effect of TRIB1 on the MAPK signaling suggests that TRIB1 alterations may be related to AML cases, which do not show any mutations in the pathway members, such as FLT3, c-Kit, or Ras. In this report, we identified a novel somatic mutation of *TRIB1* in a case of human acute megakaryocytic leukemia developed in DS (DS-AMKL). Retrovirus-mediated gene transfer followed by bone marrow transfer indicated that the mutation enhanced leukemogenic activity and MAPK phosphorylation by TRIB1.

Methods

Patients

TRIB1 mutations have been investigated in 12 cases of transient leukemia (TL), 5 of DS-AMKL, and 4 cell lines of DS-AML. Peripheral blood leukocytes of TL and bone marrow cells of DS-AMKL were used as sources for the molecular analysis. This study was approved by the Ethics Committee of Hirosaki University Graduate School of Medicine, and all clinical samples were obtained with informed consent from the parents of all patients, in accordance with the Declaration of Helsinki.

Patient 84 showed trisomy 21 and extensive leukocytosis at birth. Hematologic findings revealed the white blood cell count to be 148 × 10^9/L, including 87% myeloblasts, a hemoglobin level of 19.4 g/dL, and a platelet count of 259 × 10^9/L. Patent ductus arteriosus and atrial septal defect have been pointed out. Based on the hematologic data and the chromosomal abnormality, the patient was diagnosed as DS-related TL. The hematologic abnormality was then improved, but 8 months later 3% of 6.9 × 10^9/L white blood cells became myeloblasts (Figure 1A). A karyotype analysis of bone marrow cells revealed 48, XY,+8,+21 in 3 of 20 cells. In addition, *GATA1* mutation was detected at nt 113 from A to G, resulting in loss of the first methionine.[7] He was diagnosed as AMKL at this time, and his disease was in remission by subsequent chemotherapy.

PCR and sequencing

The entire coding region of human *TRIB1* cDNA of patients' samples was amplified using Taq polymerase (Promega) and specific primer pairs (the sequences of the primers are available on request). The genomic DNA samples of patient 84 were also analyzed. The sequence analysis of *GATA1* was performed as described previously.[7] After checking the PCR products by agarose gel electrophoresis, the products were purified and directly sequenced.

Submitted December 12, 2010; accepted January 6, 2012. Prepublished online as *Blood* First Edition paper, January 31, 2012; DOI 10.1182/blood-2010-12-324806.

The online version of this article contains a data supplement.

The publication costs of this article were defrayed in part by page charge payment. Therefore, and solely to indicate this fact, this article is hereby marked "advertisement" in accordance with 18 USC section 1734.

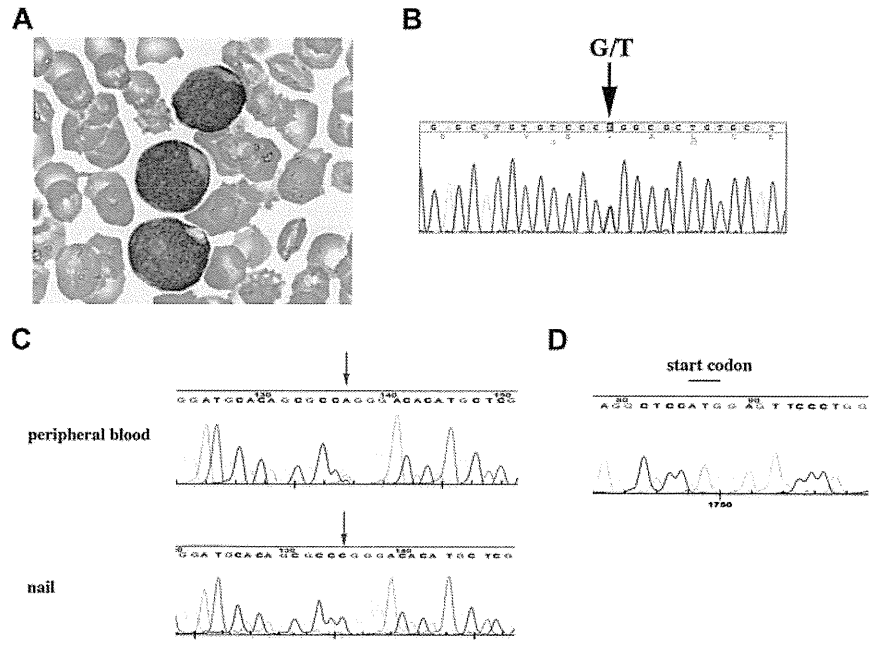

Figure 1. *TRIB1* R107L mutation identified in DS-related leukemias. (A) Giemsa staining of the case 84 peripheral blood smear diagnosed as AMKL. The image was acquired using a BX40 microscope equipped with a 100×/1.30 NA oil objective (Olympus) and a C-4040 digital camera (Olympus). (B) Fluorescent dye sequencing chromatographs of *TRIB1* genotyping by direct sequencing of the case 84 using a cDNA sample as a template. The vertical arrow indicates mixed G and T signals at codon 107. (C) Fluorescent dye sequencing chromatographs of *TRIB1* of peripheral blood leukocytes (top) or nail (bottom) in the same case at the complete remission stage. The red arrows indicate that the mutation remains in leukocytes but not in nail. The reverse strand sequences are shown. (D) *GATA1* sequence. The start codon that was mutated in AMKL[7] is normal in the peripheral blood leukocytes at the remission stage.

Retroviral infection of murine bone marrow cells and bone marrow transfer

Bone marrow cells were prepared from 8-week-old female C57Bl/6J mice 5 days after injection of 150 mg/kg body weight of 5-fluorouracil (Kyowa Hakko Kogyo). Retroviral infection of bone marrow cells and bone marrow transfer experiments were performed as described.[2] Transduction efficiencies evaluated by flow cytometric techniques were comparable between wild-type (WT; 5.3%) and R107L (3.4%). Animals were housed, observed daily, and handled in accordance with the guidelines of the animal care committee at Japanese Foundation for Cancer Research. All the diseased mice were subjected to autopsy and analyzed morphologically, and the blood was examined by flow cytometric techniques. The mice were diagnosed as positive for AML according to the classification of the Bethesda proposal.[8] The survival rate of each group was evaluated using the Kaplan-Meier method, and differences between survival curves were compared using the log-rank test.

Immunoblotting

Immunoblotting was performed using cell lysates in RIPA buffer as described.[4] Anti-p44/42 ERK (Cell Signaling Technologies), anti–phospho-p44/42 ERK (Cell Signaling Technologies), anti-C/EBPα (Santa Cruz Biotechnology), anti-FLAG (Sigma-Aldrich), and anti-GAPDH (Hy Test Ltd) antibodies were used.

Results and discussion

The important role of TRIB1 on the MAPK signaling suggests that *TRIB1* alterations may occur in some AML cases, which do not show overlapping mutations in the pathway members, such as FLT3, KIT, or RAS. Therefore, we tried to search mutations of *TRIB1* in cases of ML-DS and TL in which such mutations are infrequent.[9] In a case of DS-AMKL (case 84), a nucleotide change from guanine to thymine has been identified at 902 that results in amino acid alteration from arginine 107 (R107) to leucine (Figure 1B). The sequence changes were confirmed by subcloning the PCR product into the TA-type plasmid vector (data not shown). The nucleotide change was not observed in the DNA sample derived from the nail of the same patient at all (Figure 1C), indicating that this change is a somatic mutation. Interestingly, the mutation was retained in the peripheral blood sample in the complete remission stage in which the GATA1 mutation completely disappeared (Figure 1C-D). These results indicate that the *TRIB1* mutation precedes the onset of TL and the *GATA1* mutation, and suggest that *TRIB1* mutation occurred at the hematopoietic stem cell level and that the clone retaining the *TRIB1* mutation survived after chemotherapy. In case 84, there was no mutation for *FLT3* exons 14, 15, and 20, *PTPN11* exons 3 and 13, *KRAS* exons 2, 3, and 5, and *KIT* exons 8, 11, and 17 by the high-resolution melt analysis (data not shown).

An additional mutation was found in a case of TL (case 109) at the nucleotides 805 and 806 from GC to AT, which results in amino acid conversion from alanine (A75) to isoleucine (supplemental Figure 1, available on the *Blood* Web site; see the Supplemental Materials link at the top of the online article). *TRIB1* expression in DS-related and DS-unrelated leukemias was examined by real-time quantitative RT-PCR (supplemental Figure 2).

R107 is located within a psuedokinase domain of TRIB1 that is considered as a functionally core domain of TRIB family proteins.[10] Sequence comparison among 3 TRIB family proteins as well as tribbles homologs in other organisms revealed that the R107 is well conserved in mammalian TRIB1 and TRIB2,[10] suggesting that this arginine residue is evolutionary conserved and may be related to an important function. On the other hand, A75 is located outside of the pseudokinase domain, not conserved between human and mouse, or other tribbles homologs. Moreover, the N-terminal domain containing A75 is dispensable for the leukemogenic activity of Trib1.[4] Therefore, we tried to investigate whether the R107L mutation could affect the leukemogenic activity of *TRIB1*.

R107L was introduced into the murine *Trib1* cDNA by site-directed mutagenesis. Both WT and R107L cDNAs were subcloned into the pMYs-IRES-GFP retroviral vector and were used for retrovirus-mediated gene transfer followed by bone marrow transfer according to the method previously described.[1] All the mice

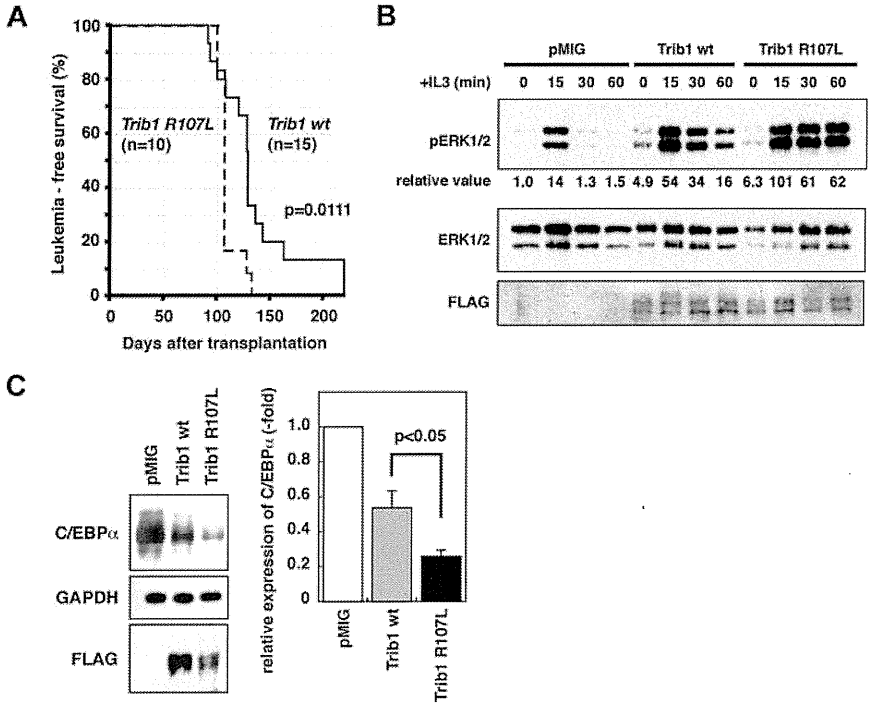

Figure 2. AML development by bone marrow transfer using *Trib1* WT and R107L. (A) Kaplan-Meier survival curves are shown. The *P* value was calculated with the log-rank test. (B) Immunoblot analysis of *Trib1* WT AML (Mac-1 56.2%, Gr-1 52.5%, $CD34^{lo}$, c-kit^{-}, Sca-1^{-}) and R107L AML (Mac-1 41.4%, Gr-1 25.2%, $Cd34^{lo}$, c-kit^{lo}, Sca-1^{-}) derived from bone marrow of recipient mice (WT #T73 and R107L #T151 in supplemental Table 1). Enhancement of ERK phosphorylation is more significant in R107L. Relative values of ERK phosphorylation were calculated by densitometric analysis. (C) Immunoblot analysis for C/EBPα of the same AML samples as in panel B. Relative expression level of C/EBPα is quantitated (right).

transplanted with bone marrow cells expressing WT (n = 15) or R107L (n = 12) developed AML (Figure 2A). The mean survival time was shorter in the recipients with R107L-expressing bone marrow cells (110 days) than those with WT (136 days; Figure 2A). The difference was significant ($P = .0111$, log-rank test). The result indicates that the R107L mutation enhances the leukemogenic activity of TRIB1. These results also suggest that *TRIB1* mutation might cooperate with *GATA1* mutation in the genesis of DS-AMKL, and that trisomy 21, *TRIB1*, and *GATA1* mutations occurred consecutively, which contributed to the multistep leukemogenic process.

We have shown that TRIB1 interacts with MEK1 and enhances phosphorylation of ERK.[2] The R107L mutant enhanced ERK phosphorylation more extensively than WT (Figure 2B) in AML cells derived from bone marrow of recipient mice, and more significant degradation of C/EBPα was induced by the R107L mutant (Figure 2C). These findings might be correlated to the enhanced leukemogenic activity of the mutant. Both R107L and WT proteins could interact with MEK1, having the binding motif in their C-termini. The residue 107 is located at subdomain II of the pseudokinase domain.[11] The mutation may affect conformation of the domain and may promote the MEK1 function on ERK, although additional studies are required to address the possibility. A recent study demonstrates that Trib1 and Trib2 failed to show ERK phosphorylation in 32D cells.[12] The different response to Trib1 between primary leukemic cells and the cell line might depend on the cellular context and/or combination of additional mutations. The AML phenotypes were somewhat varied in each case and Mac-1–positive/Gr-1–negative AMLs were more remarkable in WT than in R107L, although the difference was not statistically significant (supplemental Figures 3-4; supplemental Table 1). The current study underscores the role of TRIB1 in human leukemogenesis and the significance of the R107L mutation in its function. Further sequence analysis of tribbles family genes in a larger cohort will emphasize the importance of R107L and/or additional mutations of *TRIB1* in leukemic patients.

Acknowledgments

This work was supported by KAKENHI (Grant-in-Aid for Scientific Research) on Priority Areas Integrative Research Toward the Conquest of Cancer (E.I. and T.N.) and the Ministry of Education, Culture, Sports, Science and Technology of Japan (Young Scientists, T.Y.).

Authorship

Contribution: T.Y., E.I., Y.H., and T.N. designed and performed the research and wrote the manuscript; T. Toki, Y.A., R.K., and M.-j.P. performed the research; and Y.K., T. Takahara, and Y.Y. contributed to the bone marrow transplantation analysis.

Conflict-of-interest disclosure: The authors declare no competing financial interests.

Correspondence: Takuro Nakamura, Division of Carcinogenesis, Cancer Institute, Japanese Foundation for Cancer Research, 3-8-31 Ariake, Koto-ku, Tokyo 135-8550, Japan; e-mail: takuro-ind@umin.net.

References

1. Shimizu R, Engel JD, Yamamoto M. GATA1-related leukaemias. *Nat Rev Cancer.* 2008;8(4):279-287.
2. Jin G, Yamazaki Y, Takuwa M, et al. Trib1 and Evi1 cooperate with Hoxa and Meis1 in myeloid leukemogenesis. *Blood.* 2007;109(9):3998-4005.
3. Kiss-Toth E, Bagstaff SM, Sung HY, et al. Human Tribbles, a protein family controlling mitogen-activated protein kinase cascades. *J Biol Chem.* 2004;279(41):42703-42708.
4. Yokoyama T, Kanno Y, Yamazaki Y, et al. Trib1 links the MEK/ERK pathway in myeloid

leukemogenesis. *Blood.* 2010;116(15):2768-2775.

5. Keeshan K, He Y, Wouters BJ, et al. Tribbles homolog 2 inactivates C/EBPalpha and causes acute myelogenous leukemia. *Cancer Cell.* 2006; 10(5):401-411.
6. Storlazzi CT, Fioretos T, Surace C, et al. MYC-containing double minutes in hematologic malignancies: evidence in favor of the episome model and exclusion of MYC as the target gene. *Hum Mol Genet.* 2006;15(6):933-942.
7. Kanezaki R, Toki T, Terui K, et al. Down syndrome and GATA1 mutations in transient abnormal myeloproliferative disorder: mutation classes correlate with progression to myeloid leukemia. *Blood.* 2010;116(22):4631-4638.
8. Kogan SC, Ward JM, Anver MR, et al. Bethesda proposal for classification of nonlymphoid hematopoietic neoplasms in mice. *Blood.* 2002;100(1): 238-245.
9. Toki T, Kanezaki R, Adachi S, et al. The key role of stem cell factor/KIT signaling in the proliferation of blast cells from Down syndrome-related leukemia. *Leukemia.* 2009;23(1):95-103.
10. Hegedus Z, Czibula A, Kiss-Toth E. Tribbles: a family of kinase-like proteins with potent signaling regulatory function. *Cell Signal.* 2007;19(2):238-250.
11. Yokoyama T, Nakamura T. Tribbles in disease: signaling pathways important for cellular function and neoplastic transformation. *Cancer Sci.* 2011;102(6):1115-1122.
12. Dedhia PH, Keeshan K, Uljon S, et al. Differential ability of Tribbles family members to promote degradation of C/EBPalpha and induce acute myelogenous leukemia. *Blood.* 2010; 116(8):1321-1328.

Brief report

CBL mutation in chronic myelomonocytic leukemia secondary to familial platelet disorder with propensity to develop acute myeloid leukemia (FPD/AML)

Norio Shiba,[1,2] Daisuke Hasegawa,[3] Myoung-ja Park,[1] Chisato Murata,[1] Aiko Sato-Otsubo,[4] Chitose Ogawa,[3] Atsushi Manabe,[3] Hirokazu Arakawa,[2] Seishi Ogawa,[4] and Yasuhide Hayashi[1]

[1]Department of Hematology/Oncology, Gunma Children's Medical Center, Shibukawa, Japan; [2]Department of Pediatrics, Gunma University Graduate School of Medicine, Maebashi, Japan; [3]Department of Pediatrics, St Luke's International Hospital, Tokyo, Japan; and [4]Cancer Genomics Project, Graduate School of Medicine, University of Tokyo, Tokyo, Japan

Familial platelet disorder with a propensity to develop acute myeloid leukemia (FPD/AML) is a rare autosomal dominant disease characterized by thrombocytopenia, abnormal platelet function, and a propensity to develop myelodysplastic syndrome (MDS) and AML. So far, > 20 affected families have been reported. Recently, a second *RUNX1* alteration has been reported; however, no additional molecular abnormalities have been found so far. We identified an acquired *CBL* mutation and 11q-acquired uniparental disomy (11q-aUPD) in a patient with chronic myelomonocytic leukemia (CMML) secondary to FPD with *RUNX1* mutation but not in the same patient during refractory cytopenia. This finding suggests that alterations of the *CBL* gene and *RUNX1* gene may cooperate in the pathogenesis of CMML in patients with FPD/AML. The presence of *CBL* mutations and 11q-aUPD was an important "second hit" that could be an indicator of leukemic transformation of MDS or AML in patients with FPD/AML. (*Blood.* 2012; 119(11):2612-2614)

Introduction

Familial platelet disorder with a propensity to develop acute myeloid leukemia (FPD/AML) is a rare autosomal dominant disease characterized by thrombocytopenia, abnormal platelet function, and a propensity to develop myelodysplastic syndrome (MDS) and AML.[1,2] Since Song et al reported haploinsufficiency of the *RUNX1/CBFA2* gene,[3] more than 20 affected families have been reported.[4-8] Notably, various types of mono-allelic mutations of the *RUNX1* gene have been found in patients with AML secondary to FPD.[3,7-9] *RUNX1*, which is a key regulator of definitive hematopoiesis and myeloid differentiation, is also commonly involved in sporadic cases of MDS and AML, by translocations in AML[10] and by point mutations in AML[11,12] and MDS.[13] Recently, a second *RUNX1* alteration has been reported[8]; however, no additional molecular abnormalities have been found so far.

In this regard, recent reports of somatic mutations of the *CBL* proto-oncogene in myeloid neoplasms are intriguing because these *CBL* mutations have been shown to result in aberrant tyrosine kinase signaling, which would also lead to the activation of RAS signaling pathways. So far, we and others have reported that *CBL* mutations occurred in a variety of myeloid neoplasms, including de novo AML,[14,15] MDS,[16,17] and myeloproliferative neoplasm,[16,17] especially in chronic myelomonocytic leukemia (CMML)[16,17] and juvenile myelomonocytic leukemia.[18] The importance of *CBL* mutations for leukemogenesis has substantially increased, which prompted us to search for possible *CBL* mutations in this pedigree.

Here, we reported that *CBL* mutation developed at the time of diagnosis of CMML, but not during refractory cytopenia, in a Japanese patient with FPD/AML harboring a *RUNX1* mutation.

Methods

RUNX1 mutation analysis

DNA and RNA were extracted from peripheral blood (PB) of the proband, her sister, and their mother after obtaining informed consent. We performed mutation analysis of the *RUNX1* gene by PCR followed by direct sequencing with the use of an ABI PRISM 310 Genetic Analyzer (Applied Biosystems). For further confirmation of deletion mutations, the PCR products were subcloned with the use of a TOPO TA Cloning Kit (Invitrogen) and then sequenced. Mutations were screened from exons 1-8 of the *RUNX1* gene.

CBL mutation analysis

Because *CBL* mutations thus far reported almost exclusively involved exons 8-9 that encode Linker/RING finger domains, we confined our mutation analysis to these exons, which were subjected to direct sequencing. Because the frequency of 11q-acquired uniparental disomy (11q-aUPD) was reported as ~ 85%-90% in *CBL* mutations, we also analyzed the sample with Affymetrix GeneChip 250K *Nsp*I.[17-19] Genome-wide detection of copy number abnormalities or allelic imbalances was performed with CNAG/AsCNAR Version 3.0 software (http://www.genome.umin.jp), which enabled sensitive detection of copy number neutral loss of heterozygosity (or aUPD).[19] In addition, we examined mutations of the following genes in the proband as previously reported: *FLT3, KIT, RAS, JAK2, PTPN11, ASXL1, IDH1/2,* and *MPL*.[20-22] The study adhered to the principles of the Helsinki Declaration and was conducted under the regulations enacted by the Ethics Board of Gunma Children's Medical Center.

Results and discussion

The proband (III-2), who was the second child of nonconsanguineous parents, underwent an 8-year follow-up of mild to moderate

Submitted February 2, 2011; accepted November 24, 2011. Prepublished online as *Blood* First Edition paper, December 2, 2011; DOI 10.1182/blood-2011-02-333435.

The publication costs of this article were defrayed in part by page charge payment. Therefore, and solely to indicate this fact, this article is hereby marked "advertisement" in accordance with 18 USC section 1734.

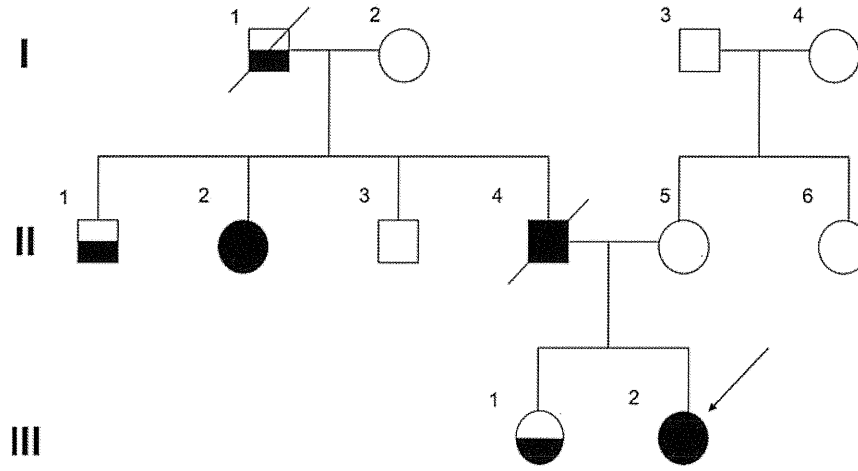

Figure 1. The family pedigree. Squares indicate males and circles indicate females. Open symbols represent unaffected persons, half-filled symbols represent persons affected by thrombocytopenia, and closed symbols represent persons affected by FPD who developed MDS/AML. The proband (III-2) is indicated by an arrow.

thrombocytopenia (50-80 × $10^3/\mu L$), and at that age of 10 years, her condition was diagnosed as refractory cytopenia. Cytogenetic analysis found a normal karyotype, and FISH showed neither monosomy 7 nor trisomy 8. The proband had been closely observed without any therapy for 2 years and 9 months because she did not require transfusion and her disease remained stable; however, at the age of 12 years, leukocytosis and monocytosis developed and she became dependent on platelet transfusions. Finally, the disease evolved to CMML, and allogeneic bone marrow (BM) transplantation from an unrelated donor was performed. During the entire course, the number of blast cells in PB was constantly < 2%, and no additional symptoms were observed, such as hepatosplenomegaly. Her elder sister (III-1) was also followed for 10 years with mild thrombocytopenia; however, the morphologic findings of PB or BM were not compatible with myeloproliferative neoplasms.[17] Because her platelet count has been gradually decreasing, allogeneic BM transplantation is being considered. Although her father (II-4) developed MDS at the age of 41 and died 2 years later, her paternal aunt (II-2) developed MDS at the age of 49 and has remained in complete remission for 11 years after successful allogeneic cord blood transplantation. Her paternal grandfather (I-1) and uncle (II-1) also had a history of thrombocytopenia (Figure 1). Direct sequencing analysis of *RUNX1* found a one-base deletion of adenine at position 2364 within exon 7, resulting in a frameshift mutation that corresponded to AML1b transcript in the proband and her sister (Figure 2A). This resulted in a frameshift after amino acid change G262GfsX21. This mutation was not detected in their mother. All these data suggested that her paternal grandfather (I-1), uncle (II-1), aunt (II-2), and her father (II-4) were considered to have FPD/AML, carrying the same *RUNX1* mutation.

Although no *CBL* mutations were found in the proband sample of refractory cytopenia before development of CMML, homozygous mutation of the *CBL*, which was located in the splice acceptor site of intron 8 (Figure 2B), was identified in the proband sample in the CMML. We also found 11q-aUPD (Figure 2C) in the proband sample, confirming a strong association of *CBL* mutations with 11q-aUPD, as previously described[16-18]; however, no mutations of any other genes, including *FLT3*, *KIT*, *RAS*, *JAK2*, *PTPN11*, *ASXL1*, *IDH1/2*, and *MPL*, were found and no additional somatic *RUNX1* alterations. No *CBL* mutations were found in her sister's sample at this time.

Inherited *RUNX1* mutations were clustered in the N-terminal region in exons 3-5, which affect the runt homology domain. Mutations in the C-terminal region, detected in the present pedigree, have been reported less frequently so far and are considered to affect the transactivation domain (Figure 2D).

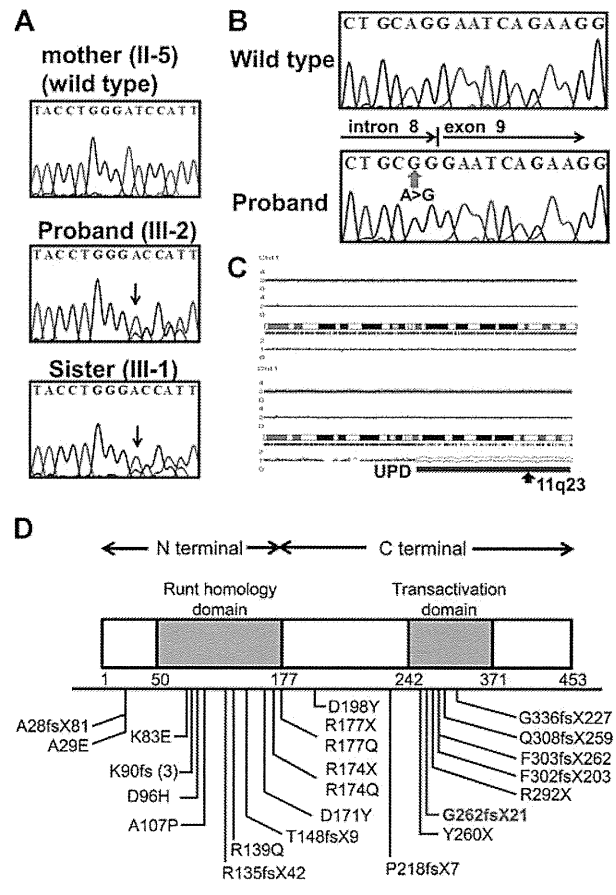

Figure 2. Mutation analysis of *RUNX1* and *CBL* genes in the pedigree. (A) Direct sequencing analysis of affected patients (III-1, III-2) and an unaffected family member (II-5) is shown. Arrow indicates a one-base deletion of adenine. (B) Mutated *CBL* is shown in the proband. (C) Identification of acquired uniparental disomy of 11q in the proband. Total copy number (tCN; red plot) is shown above the cytoband, and the results of allele-specific copy number analysis with anonymous references (AsCNAR) plots are shown below the cytoband. Larger allele is presented by a red line, and the smaller allele is presented by a blue line. Allele-specific analysis showed 11q-aUPD (blue line), which contained the *CBL* region (arrow). (D) Schematic representation of wild-type and mutated *RUNX1*. The affected *RUNX1* is truncated at the C terminus of the transactivation domain (TAD). Part of TAD is lacking in this proband (red line).

It has been postulated that disruption of the *RUNX1* gene is not sufficient to cause AML, as previously reported with monoallelic and biallelic inactivation of *Runx1* in mice[23,24] and in mice carrying the knocked-in *Runx1-Eto* chimeric gene. These data indicate that a second-hit mutation in addition to the dysfunction of *RUNX1* is required for the development of AML. Minelli et al postulated that the mutations seen in FPD cases have a mutation effect that induces additional genetic abnormalities and promotes progression to hematologic malignancies.[25]

Marked associations between chromosome translocation and gene mutations have been reported: *KIT* mutation in core binding leukemia, t(8;21)/*AML1-ETO* and inv(16)(p13q22)/*CBFβ-MYH11*, *FLT3*-ITD in leukemia with t(15;17)/*PML-RARα*, or with t(6;9)/*DEK-CAN*. We consider that it is important to find an association to administer clinically relevant treatment. In addition to the germline *RUNX1* mutation, we identified an acquired *CBL* mutation in the proband and assumed it to be a second hit mutation by which FPD evolved into CMML. To our knowledge, this is the first patient with FPD/AML in whom *CBL* mutation has developed. This finding suggests that alterations of the *CBL* gene and *RUNX1* could cooperate in the pathogenesis of CMML or AML in patients with FPD/AML. The presence of 11q-aUPD provided evidence that loss of the wild-type copy of *CBL* with duplication of the mutant copy was an important second hit that could be an indicator of leukemic transformation in patients with FPD/AML.

Acknowledgments

The authors thank Miss Sayaka Takeuchi for her excellent technical assistance.

This work was supported by a grant for cancer research and a grant for research on children and families from the Ministry of Health, Labor, and Welfare of Japan; a Grant-in-Aid for Scientific Research (B, C) and Exploratory Research from the Ministry of Education, Culture, Sports, Science, and Technology of Japan; and by a research grant for Gunma Prefectural Hospitals.

Authorship

Contribution: Y.H. and C.O. designed the study; A.M., C.O., and D.H. provided critical reagents and samples; N.S., M.P., A.S.-O., and C.M. performed the experiments; H.A. and S.O. supervised the work; N.S. and M.P. analyzed the results; N.S. and D.H. constructed the figures; N.S. and Y.H. wrote the paper; and all the authors critically reviewed and revised the manuscript.

Conflict-of-interest disclosure: The authors declare no competing financial interests.

Correspondence: Yasuhide Hayashi, Department of Hematology/Oncology, Gunma Children's Medical Center, 779, Shimohakoda, Hokkitsu, Shibukawa, Gunma, 377-8577, Japan; e-mail: hayashiy-tky@umin.ac.jp.

References

1. Dowton SB, Beardsley D, Jamison D, Blattner S, Li FP. Studies of a familial platelet disorder. *Blood.* 1985;65(3):557-563.
2. Ho CY, Otterud B, Legare RD, et al. Linkage of a familial platelet disorder with a propensity to develop myeloid malignancies to human chromosome 21q22.1-22.2. *Blood.* 1996;87(12):5218-5224.
3. Song WJ, Sullivan MG, Legare RD, et al. Haploinsufficiency of CBFA2 causes familial thrombocytopenia with propensity to develop acute myelogenous leukaemia. *Nat Genet.* 1999;23(2):166-175.
4. Buijs A, Poddighe P, van Wijk R, et al. A novel CBFA2 single-nucleotide mutation in familial platelet disorder with propensity to develop myeloid malignancies. *Blood.* 2001;98(9):2856-2858.
5. Michaud J, Wu F, Osato M, et al. In vitro analyses of known and novel RUNX1/AML1 mutations in dominant familial platelet disorder with predisposition to acute myelogenous leukemia: implications for mechanisms of pathogenesis. *Blood.* 2002;99(4):1364-1372.
6. Owen CJ, Toze CL, Koochin A, et al. Five new pedigrees with inherited RUNX1 mutations causing familial platelet disorder with propensity to myeloid malignancy. *Blood.* 2008;112(12):4639-4645.
7. Kirito K, Sakoe K, Shinoda D, Takiyama Y, Kaushansky K, Komatsu N. A novel RUNX1 mutation in familial platelet disorder with propensity to develop myeloid malignancies. *Haematologica.* 2008;93(1):155-156.
8. Preudhomme C, Renneville A, Bourdon V, et al. High frequency of RUNX1 biallelic alteration in acute myeloid leukemia secondary to familial platelet disorder. *Blood.* 2009;113(22):5583-5587.
9. Heller PG, Glembotsky AC, Gandhi MJ, et al. Low Mpl receptor expression in a pedigree with familial platelet disorder with predisposition to acute myelogenous leukemia and a novel AML1 mutation. *Blood.* 2005;105(12):4664-4670.
10. Miyoshi H, Shimizu K, Kozu T, Maseki N, Kaneko Y, Ohki M. t(8;21) breakpoints on chromosome 21 in acute myeloid leukemia are clustered within a limited region of a single gene, AML1. *Proc Natl Acad Sci U S A.* 1991;88(23):10431-10434.
11. Osato M, Asou N, Abdalla E, et al. Biallelic and heterozygous point mutations in the runt domain of the AML1/PEBP2alphaB gene associated with myeloblastic leukemias. *Blood.* 1999;93(6):1817-1824.
12. Taketani T, Taki T, Takita J, et al. AML1/RUNX1 mutations are infrequent, but related to AML-M0, acquired trisomy 21, and leukemic transformation in pediatric hematologic malignancies. *Genes Chromosomes Cancer.* 2003;38(1):1-7.
13. Harada H, Harada Y, Niimi H, et al. High incidence of somatic mutations in the AML1/RUNX1 gene in myelodysplastic syndrome and low blast percentage myeloid leukemia with myelodysplasia. *Blood.* 2004;103(6):2316-2324.
14. Sargin B, Choudhary C, Crosetto N, et al. Flt3-dependent transformation by inactivating c-Cbl mutations in AML. *Blood.* 2007;110(3):1004-1012.
15. Caligiuri MA, Briesewitz R, Yu J, et al. Novel c-CBL and CBL-b ubiquitin ligase mutations in human acute myeloid leukemia. *Blood.* 2007;110(3):1022-1024.
16. Dunbar AJ, Gondek LP, O'Keefe CL, et al. 250K single nucleotide polymorphism array karyotyping identifies acquired uniparental disomy and homozygous mutations, including novel missense substitutions of c-Cbl, in myeloid malignancies. *Cancer Res.* 2008;68(24):10349-10357.
17. Sanada M, Suzuki T, Shih LY, et al. Gain-of-function of mutated C-CBL tumour suppressor in myeloid neoplasms. *Nature.* 2009;460(7257):904-908.
18. Shiba N, Kato M, Park MJ, et al. CBL mutations in juvenile myelomonocytic leukemia and pediatric myelodysplastic syndrome. *Leukemia.* 2010;24(5):1090-1092.
19. Nannya Y, Sanada M, Nakazaki K, et al. A robust algorithm for copy number detection using high-density oligonucleotide single nucleotide polymorphism genotyping arrays. *Cancer Res.* 2005;65(14):6071-6079.
20. Pardanani AD, Levine RL, Lasho T, et al. MPL515 mutations in myeloproliferative and other myeloid disorders: a study of 1182 patients. *Blood.* 2006;108(10):3472-3476.
21. Rocquain J, Carbuccia N, Trouplin V, et al. Combined mutations of ASXL1, CBL, FLT3, IDH1, IDH2, JAK2, KRAS, NPM1, NRAS, RUNX1, TET2 and WT1 genes in myelodysplastic syndromes and acute myeloid leukemias. *BMC Cancer.* 2010;10:401.
22. Tartaglia M, Niemeyer CM, Fragale A, et al. Somatic mutations in PTPN11 in juvenile myelomonocytic leukemia, myelodysplastic syndromes and acute myeloid leukemia. *Nat Genet.* 2003;34(2):148-150.
23. Sun W, Downing JR. Haploinsufficiency of AML1 results in a decrease in the number of LTR-HSCs while simultaneously inducing an increase in more mature progenitors. *Blood.* 2004;104(12):3565-3572.
24. Ichikawa M, Asai T, Saito T, et al. AML-1 is required for megakaryocytic maturation and lymphocytic differentiation, but not for maintenance of hematopoietic stem cells in adult hematopoiesis. *Nat Med.* 2004;10(3):299-304.
25. Minelli A, Maserati E, Rossi G, et al. Familial platelet disorder with propensity to acute myelogenous leukemia: genetic heterogeneity and progression to leukemia via acquisition of clonal chromosome anomalies. *Genes Chromosomes Cancer.* 2004;40(3):165-171.

nature immunology

The kinase Btk negatively regulates the production of reactive oxygen species and stimulation-induced apoptosis in human neutrophils

Fumiko Honda[1], Hirotsugu Kano[2], Hirokazu Kanegane[3], Shigeaki Nonoyama[4], Eun-Sung Kim[5], Sang-Kyou Lee[5], Masatoshi Takagi[1], Shuki Mizutani[1] & Tomohiro Morio[1]

The function of the kinase Btk in neutrophil activation is largely unexplored. Here we found that Btk-deficient neutrophils had more production of reactive oxygen species (ROS) after engagement of Toll-like receptors (TLRs) or receptors for tumor-necrosis factor (TNF), which was associated with more apoptosis and was reversed by transduction of recombinant Btk. Btk-deficient neutrophils in the resting state showed hyperphosphorylation and activation of phosphatidylinositol-3-OH kinase (PI(3)K) and protein tyrosine kinases (PTKs) and were in a 'primed' state with plasma membrane–associated GTPase Rac2. In the absence of Btk, the adaptor Mal was associated with PI(3)K and PTKs at the plasma membrane, whereas in control resting neutrophils, Btk interacted with and confined Mal in the cytoplasm. Our data identify Btk as a critical gatekeeper of neutrophil responses.

Among 'professional' phagocytes with a sophisticated arsenal of microbicidal features, neutrophils are the dominant cells that mediate the earliest innate immune responses to microbes[1–3]. Neutrophils migrate to the site of infection, sense and engulf microorganisms, produce reactive oxygen species (ROS) and kill the invading microbes via ROS by acting together with antimicrobial proteins and peptides[1,2]. The enzyme responsible for the respiratory burst is NADPH oxidase, which catalyzes the production of superoxide from oxygen and NADPH. This enzyme is a multicomponent complex that consists of membrane-bound flavocytochrome b_{558} (gp91^{phox} and p22^{phox}), cytosolic components (p47^{phox}, p67^{phox} and p40^{phox}) and a GTPase (Rac1 or Rac2)[3–6]. Activation of NADPH oxidase is strictly regulated both temporally and spatially to ensure that the reaction takes place rapidly at the appropriate cellular localization. Activation of this system requires three signaling triggers, including protein kinases, lipid-metabolizing enzymes and nucleotide-exchange factors that activate the Rac GTPase[3–6].

Inadequate production of ROS is associated with various human pathological conditions. Deficiency of any component of the NADPH oxidase complex results in chronic granulomatous disease, in which bacterial and fungal infections are recurrent and life-threatening[4]. Abnormalities in the molecules involved in the signal-transduction pathway initiated by the recognition of pathogen-associated molecular patterns are accompanied by less production of ROS after exposure to specific stimuli and by susceptibility to bacterial infection. These abnormalities include deficiency in the kinase IRAK4, the adaptor MyD88 deficiency or the kinase NEMO (IKKγ)[7]. In contrast, many other human disorders are believed to be associated with or induced by excessive production of ROS that causes DNA damage, tissue damage, cellular apoptosis and neutropenia[8,9].

Here we focus on determining the role of the kinase Btk in production of ROS and cellular apoptosis in human neutrophils, as 11–30% of patients with X-linked agammaglobulinemia (XLA), a human disease of Btk deficiency, have neutropenia[10,11], and Btk is a critical signaling component of phagocytic cells[12–14]. The neutropenia of XLA is distinct from that of common variable immunodeficiency (CVID) in that the neutropenia is induced by infection, is usually ameliorated after supplementation with immunoglobulin and is not mediated by the autoimmune response[10,11,14]. Although a few reports have suggested that myeloid differentiation is impaired in mice with X-linked immunodeficiency[15,16], the reason for the infection-triggered neutropenia is unknown. The role of Btk in human neutrophils remains largely unexplored.

Btk is a member of the Tec-family kinases (TFKs) that are expressed in hematopoietic cells such as B cells, monocytes, macrophages and neutrophils[12]. It has a crucial role in cell survival, proliferation, differentiation and apoptosis, especially in cells of the B lineage. In humans with XLA, B cells fail to reach maturity and are presumably doomed to premature death by the *BTK* mutation that leads to the XLA phenotype[17]. Both mice with X-linked immunodeficiency that have natural mutations in *Btk* and mice in which *Btk* is targeted have B cell defects, but these are associated with much milder effects than those seen in XLA, which suggests species differences in the role of Btk[18,19].

[1]Department of Pediatrics and Developmental Biology, Tokyo Medical and Dental University Graduate School of Medical and Dental Sciences, Tokyo, Japan. [2]Department of Pediatrics, Teikyo University School of Medicine Hospital, Mizonokuchi, Kawasaki, Japan. [3]Department of Pediatrics, Toyama University School of Medicine, Toyama, Japan. [4]Department of Pediatrics, National Defense Medical College, Tokorozawa, Japan. [5]Department of Biotechnology, College of Life Science and Biotechnology, Yonsei University, Seoul, Republic of Korea. Correspondence should be addressed to T.M. (tmorio.ped@tmd.ac.jp).

Received 28 November 2011; accepted 12 January 2012; published online 26 February 2012; doi:10.1038/ni.2234

Btk is also an important signaling component of the innate immune system in phagocytic cells. Btk is involved in signaling via Toll-like receptors (TLRs) such as TLR2, TLR4, TLR7, TLR8 and TLR9, and is associated with the TLR adaptors MyD88, Mal (TIRAP) and IRAK1 (refs. 12–14,20–22). Defective innate immune responses have been observed in monocytes, dendritic cells, neutrophils and mast cells from Btk-deficient mice[12,14]. Neutrophils from mice with X-linked immunodeficiency have poor production of ROS and nitric oxide[15].

The contribution of Btk to the human innate immune system is less obvious. Stimulation via TLR2, TLR4, TLR7-TLR8 or TLR3 results in impaired production of tumor-necrosis factor (TNF) by dendritic cells from patients with XLA, whereas the TLR4-induced production of TNF and interleukin 6 (IL-6) by monocytes from patients with XLA remains intact[23–25]. Neutrophils from control subjects and patients with XLA show no substantial differences in their phosphorylation of the mitogen-activated protein kinases p38, Jnk and Erk induced by engagement of TLR4 or TLR7-TLR8 or production of ROS induced by the same stimuli[26].

Here we evaluate the role of Btk in the production of ROS and cellular apoptosis in human neutrophils through the use of Btk-deficient neutrophils, a protein-delivery system based on a cell-permeable peptide, and specific kinase inhibitors. Unexpectedly, and in contrast to published observations of mice with X-linked immunodeficiency[15], the production of ROS was substantially augmented in the absence of Btk in neutrophils stimulated via TLRs, the TNF receptor or phorbol 12-myristate 13-acetate (PMA) but not in monocytes or in lymphoblastoid B cell lines transformed by Epstein-Barr virus. Excessive production of ROS was associated with neutrophil apoptosis, which was reversed by the transduction of wild-type Btk protein. Btk-deficient neutrophils showed activation of key signaling molecules involved in the activation of NADPH oxidase, and this was accompanied by targeting of Rac2 to the plasma membrane. Mal was confined to the cytoplasm in association with Btk but was translocated to plasma membrane and interacted with protein tyrosine kinases (PTKs) and phosphatidylinositol-3-OH kinase (PI(3)K) in the absence of Btk. Here we present our findings on the mechanism by which Btk regulates the priming of neutrophils and the amplitude of the neutrophil response.

RESULTS

Excessive production of ROS in Btk-deficient neutrophils

To investigate the production of ROS in the absence of Btk, we monitored ROS in neutrophils, monocytes and Epstein-Barr virus–transformed lymphoblastoid B cell lines obtained from patients with XLA, healthy controls and patients with CVID (disease control) by staining with dihydrorhodamine 123 (DHR123) and a luminol chemiluminescence assay. PMA-driven production of ROS in Btk-deficient neutrophils was three to four times greater than that in neutrophils from healthy controls or patients with CVID, and we observed augmented production of ROS with a suboptimal dose of PMA, whereas the baseline production of ROS was similar (**Fig. 1a–d**). Similarly, and in contrast to published reports[26], engagement of TLR2 (with its ligand tripalmitoyl cysteinyl seryl tetralysine lipopeptide (Pam_3CSK_4)), TLR4 (with its ligand lipopolysaccharide) or the TNF receptor (with TNF) followed by stimulation with formyl-Met-Leu-Phe (fMLP), an agonist of G protein–coupled receptors, elicited augmented ROS responses in neutrophils from patients with XLA (**Fig. 1e,f**). The production of ROS was minimal after stimulation with the TLR9 agonist CpG-A in neutrophils from patients with XLA and was not significantly different from that of neutrophils from healthy controls. The observed phenomena were reproduced in Btk-deficient eosinophils but not in monocytes or Epstein-Barr virus–transformed lymphoblastoid B cell lines obtained from patients with XLA (**Supplementary Fig. 1**). These data indicated Btk-deficient neutrophils had excessive NADPH oxidase activity after various stimuli.

Augmented apoptosis in Btk-deficient neutrophils

Because high ROS concentrations are potentially harmful to cells, we investigated cell death induced by various stimuli in neutrophils from patients with XLA by staining with annexin V and the membrane-impermeable DNA-intercalating dye 7-AAD. Stimulation with PMA, TLR agonist plus fMLP, or TNF plus fMLP induced a significantly higher frequency of cells positive for annexin V among neutrophils from patients with XLA than among control neutrophils, whereas spontaneous cell death in the absence of stimulation was not significantly altered at 4 h in neutrophils from healthy controls versus those from patients with XLA (**Fig. 2a,b**). We observed cleavage of caspase-3, lower mitochondrial membrane potentials and degradation of proliferating

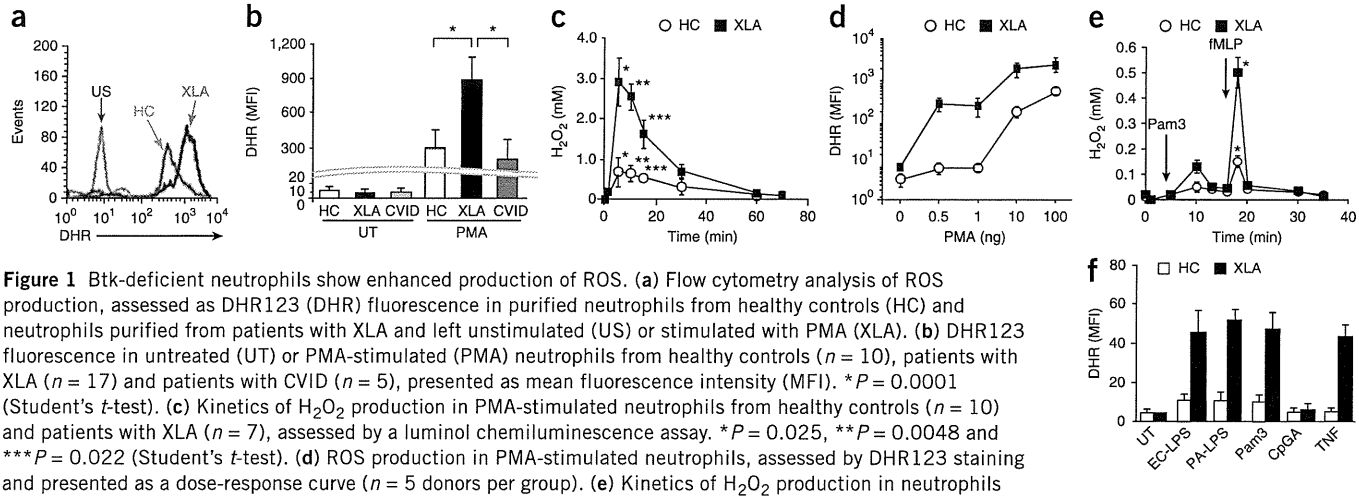

Figure 1 Btk-deficient neutrophils show enhanced production of ROS. (**a**) Flow cytometry analysis of ROS production, assessed as DHR123 (DHR) fluorescence in purified neutrophils from healthy controls (HC) and neutrophils purified from patients with XLA and left unstimulated (US) or stimulated with PMA (XLA). (**b**) DHR123 fluorescence in untreated (UT) or PMA-stimulated (PMA) neutrophils from healthy controls ($n = 10$), patients with XLA ($n = 17$) and patients with CVID ($n = 5$), presented as mean fluorescence intensity (MFI). $^*P = 0.0001$ (Student's t-test). (**c**) Kinetics of H_2O_2 production in PMA-stimulated neutrophils from healthy controls ($n = 10$) and patients with XLA ($n = 7$), assessed by a luminol chemiluminescence assay. $^*P = 0.025$, $^{**}P = 0.0048$ and $^{***}P = 0.022$ (Student's t-test). (**d**) ROS production in PMA-stimulated neutrophils, assessed by DHR123 staining and presented as a dose-response curve ($n = 5$ donors per group). (**e**) Kinetics of H_2O_2 production in neutrophils stimulated with Pam_3CSK_4 (Pam3) and fMLP, assessed by a luminol chemiluminescence assay ($n = 7$ donors per group). $^*P = 0.005$ (Student's t-test). (**f**) DHR123 fluorescence in neutrophils incubated with lipopolysaccharide from *Escherichia coli* (EC-LPS) or *Pseudomonas aeruginosa* (PA-LPS), Pam_3CSK_4, CpG-A or TNF, followed by stimulation with fMLP ($n = 7$ donors per group). Data are representative of seventeen experiments (**a**) or are pooled from at least five (**b**,**c**,**e**,**f**) or four (**d**) independent experiments (mean and s.d. in **b**–**f**).

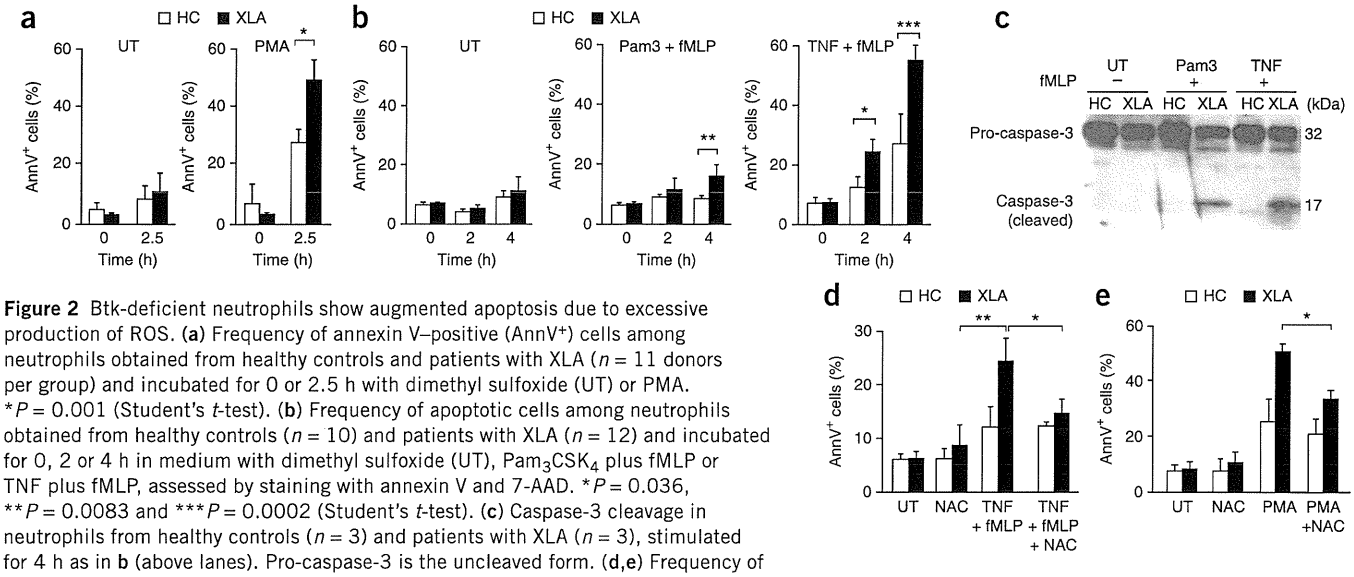

Figure 2 Btk-deficient neutrophils show augmented apoptosis due to excessive production of ROS. (**a**) Frequency of annexin V–positive (AnnV$^+$) cells among neutrophils obtained from healthy controls and patients with XLA ($n = 11$ donors per group) and incubated for 0 or 2.5 h with dimethyl sulfoxide (UT) or PMA. $^*P = 0.001$ (Student's *t*-test). (**b**) Frequency of apoptotic cells among neutrophils obtained from healthy controls ($n = 10$) and patients with XLA ($n = 12$) and incubated for 0, 2 or 4 h in medium with dimethyl sulfoxide (UT), Pam_3CSK_4 plus fMLP or TNF plus fMLP, assessed by staining with annexin V and 7-AAD. $^*P = 0.036$, $^{**}P = 0.0083$ and $^{***}P = 0.0002$ (Student's *t*-test). (**c**) Caspase-3 cleavage in neutrophils from healthy controls ($n = 3$) and patients with XLA ($n = 3$), stimulated for 4 h as in **b** (above lanes). Pro-caspase-3 is the uncleaved form. (**d**,**e**) Frequency of apoptotic Btk-deficient neutrophils ($n = 5$ donors) stimulated for 2 h (**d**) or 2.5 h (**e**) with the antioxidant N-acetyl-cysteine (NAC). $^*P = 0.043$ and $^{**}P = 0.036$ (**d**) or $^*P = 0.026$ (**e**; Student's *t*-test). Data are representative of three experiments (**b**) or at least five independent experiments (**a**,**c**–**e**; mean and s.d. in **a**,**b**,**d**,**e**).

cell nuclear antigen; hence, cell death was caused by apoptosis (**Fig. 2c** and **Supplementary Fig. 2**). Apoptosis assessed by these methods was augmented considerably for neutrophils from patients with XLA. The observed apoptosis was most probably triggered by ROS, as coincubation of neutrophils with N-acetyl cysteine, an antioxidant, rescued the cells from apoptosis induced by TNF plus fMLP or by PMA (**Fig. 2d**,**e**). We detected much more ROS release and stimulation-induced apoptosis of neutrophils from all patients with XLA regardless of the site or mode of their mutation (**Supplementary Fig. 3**). In addition, we found no correlation between genotype and the extent of neutrophil production of ROS. These data suggested that neutrophils from patients with XLA are susceptible to apoptosis triggered by pathogens.

Normalization of the ROS response by transduction of Btk

We next determined whether the enhanced apoptosis noted above was due to a defect in Btk itself or abnormal myeloid differentiation in the absence of Btk. For this, we prepared three recombinant Btk proteins (full-length Btk; Btk with deletion of the pleckstrin homology (PH) domain; and Btk with deletion of the kinase domain) fused to the cell-permeable peptide Hph-1 (**Fig. 3a**,**b**). We purified the products and transduced the proteins into neutrophils lacking Btk. The efficacy of transduction was more than 95%; and Hph-1–Btk expression was stable for at least 12–24 h (ref. 27). We adjusted the expression of Btk to that in neutrophils from healthy controls by incubating 1×10^6 cells for 1 h with 1 μM recombinant fusion protein. Transduction of full-length Btk into neutrophils from patients with XLA restored the production of ROS and the frequency of apoptotic cells after PMA stimulation to that observed for neutrophils from healthy controls (**Fig. 3c**,**d**). Transduction of the recombinant fusion of Btk with deletion of the PH domain only modestly reversed neutrophil overactivation (**Fig. 3c**), which indicated that appropriate cellular localization and interactions with other molecules were required for Btk function. Transduction of the recombinant fusion of Btk with deletion of the kinase domain minimally corrected excessive production of ROS (**Fig. 3c**), which suggested that the kinase activity of Btk or molecules that interacted via the kinase domain were critical for the regulation of ROS. We also confirmed the importance of the kinase domain by an experiment that showed excessive production of ROS in normal neutrophils treated with 50 μM LFM-A13, an inhibitor of the kinase activity of Btk, but not in those treated with LFM-A11, a control compound (**Fig. 3e**). We also documented augmented apoptosis in control neutrophils treated with LFM-A13 (**Fig. 3f**). These data demonstrated that the enhanced production of ROS and apoptosis was directly related to a defect in Btk.

NADPH oxidase components in Btk-deficient neutrophils

The NADPH oxidase complex consists of the transmembrane component (gp91^{phox} and p22^{phox}), a cytosolic component (p47^{phox}, p67^{phox} and p40^{phox}) and Rac2 (refs. 3–6). The activity of NADPH oxidase is controlled by targeting of the cytosolic components to the plasma membrane or phosphorylation of the cytosolic components or both. To assess the mechanism of the excessive production of ROS in Btk-deficient neutrophils, we investigated the abundance, phosphorylation and subcellular localization of each component by immunoblot analysis.

The expression of each component of the NADPH oxidase complex was similar in neutrophils from patients with XLA and those from healthy controls (**Fig. 4a**). The amount of p47^{phox}, p67^{phox} and p40^{phox} in the cytoplasm and the membrane was not substantially different in neutrophils from patients with XLA and those from healthy controls (**Fig. 4b**). Similarly, the amount in the membrane-targeted fraction after stimulation with PMA was not very different in neutrophils from patients with XLA and those from healthy controls (**Fig. 4c**). Phosphorylation of Ser345 in p47^{phox} and of Thr154 in p40^{phox} are important for translocation of the cytosolic components to the membrane[4,5,28]. Those modifications were not altered in Btk-deficient neutrophils (**Fig. 4c**). In contrast, we detected Rac2 in the plasma membrane of Btk-deficient neutrophils before stimulation with PMA. We observed four- to fivefold higher membrane expression of Rac2 in neutrophils from patients with XLA than in those from healthy controls in the resting state (**Fig. 4b**).

Typically, 10–15% of gp91^{phox} is located in the plasma membrane of unstimulated neutrophils, whereas the majority of the molecule resides in specific granules. Membrane expression increases after

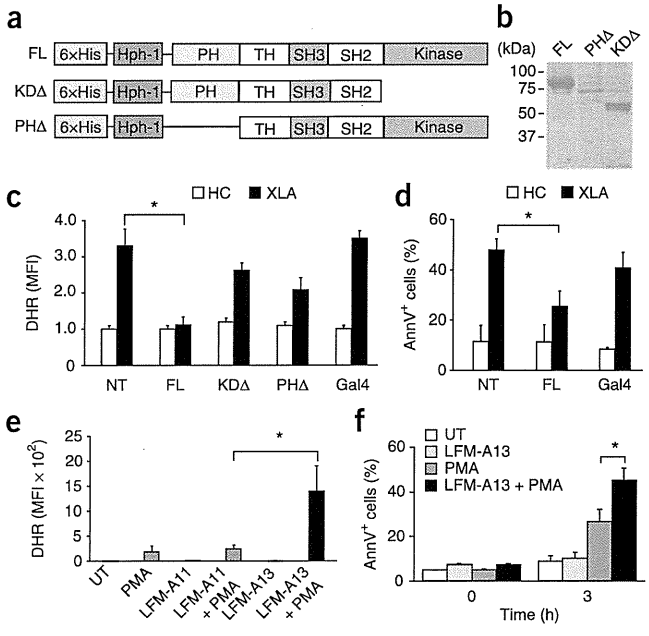

Figure 3 Excessive production of ROS and apoptosis in neutrophils from patients with XLA are abrogated by transduction of Hph-1–tagged full-length recombinant Btk but not by Hph-1–tagged Btk with deletion of the kinase or PH domain. (**a**) Hph-1–tagged Btk constructs: full-length Btk (FL); Btk with deletion of the kinase domain (KDΔ); Btk with deletion of the PH domain (PHΔ). 6×His, six-histidine tag; TH, Tec homology; SH3, Src homology 3; SH2, Src homology 2. (**b**) Size of purified Hph-1–tagged Btk proteins, confirmed by Coomassie brilliant blue staining. (**c**) ROS production in neutrophils from healthy controls ($n = 5$) and patients with XLA ($n = 5$), left untransduced (NT) or transduced with the constructs in **a** or Hph-1–tagged yeast transcriptional activator Gal4 (far right; control), presented as the MFI of DHR123 relative to that of untreated neutrophils from healthy controls, set as 1. (**d**) Frequency of apoptotic cells among neutrophils from healthy controls and patients with XLA, left untransduced or transduced with Hph-1–tagged full-length Btk or Gal4 (control). (**e**) DHR123 fluorescence in neutrophils from healthy controls ($n = 7$) left untreated or treated with PMA alone, or pretreated with LFM-A13 (Btk inhibitor) or LFM-A11 (control) alone or followed by stimulation with PMA (+ PMA). (**f**) Frequency of annexin V–positive cells among neutrophils from healthy controls ($n = 7$) left untreated or treated with PMA alone, or pretreated with LFM-A13 (50 μM, a concentration that does not inhibit other PTKs[47,48]) alone or followed by stimulation with PMA. $^*P = 0.0021$ (**c**), 0.019 (**d**), 0.021 (**e**) or 0.025 (**f**; Student's *t*-test). Data are representative of five experiments (**b**) or are pooled from six (**c**), three (**d**) or four (**e**,**f**) independent experiments (mean and s.d. in **c**–**f**).

signaling via TLRs or G protein–coupled receptors because of translocation to the plasma membrane[2]. Immunoblot analysis with antibody to gp91 (anti-gp91; **Fig. 4b**) and flow cytometry analysis of surface flavocytochrome b_{558} (**Fig. 4d**) showed higher gp91 expression in neutrophils from patients with XLA. Immunohistochemical analysis by confocal fluorescence microscopy showed localization of gp91 and Rac2 together in the membranes of resting Btk-deficient neutrophils but not in neutrophils from healthy controls (**Fig. 4e**). These results suggested that NADPH oxidase complex was partially assembled and ready to be activated in steady-state Btk-deficient neutrophils.

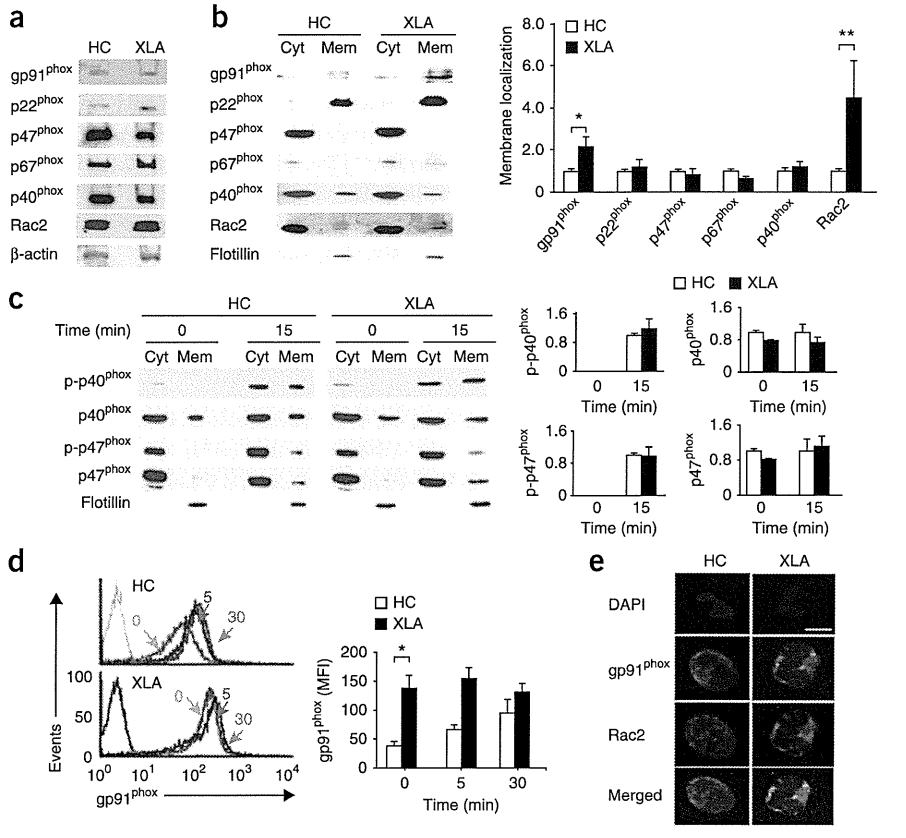

Figure 4 Btk-deficient neutrophils show targeting of Rac2 to the plasma membrane, colocalization of Rac2 with gp91^{phox} and higher membrane expression of gp91^{phox}. (**a**) Immunoblot analysis of the components of the NADPH oxidase complex in neutrophils from a healthy control and a patient with XLA. β-actin serves as a loading control throughout. (**b**) Immunoblot analysis (left) of the components of the NADPH oxidase complex in the cytoplasm (Cyt) and plasma membrane (Mem) of neutrophils from healthy controls and patients with XLA ($n = 9$ per group). Right, quantification of the membrane expression at left, presented as band intensity relative to that of flotillin (loading marker for the membrane-raft fraction) in membranes of neutrophils from healthy controls, set as 1. $^*P = 0.045$ and $^{**}P = 0.027$ (Student's *t*-test). (**c**) Immunoblot analysis of total and phosphorylated (p-) p40^{phox} and p47^{phox} in the cytoplasm and membrane of PMA-stimulated neutrophils from healthy controls and patients with XLA. Right, quantification as in **b**. (**d**) Flow cytometry analysis of gp91^{phox} on neutrophils from healthy controls and patients with XLA, left unstimulated (0) or stimulated for 5 or 30 min (above lines) with PMA, detected by staining with mAb 7D5 to gp91. Gray lines indicate staining with MsIgG (control). Right, quantification of the gp91 MFI in cells treated as at left. $^*P = 0.0039$ (Student's *t*-test). (**e**) Confocal microscopy of gp91^{phox} (green) and Rac2 (red) in healthy controls and neutrophils from patients with XLA; nuclei are counterstained with the DNA-intercalating dye DAPI (blue). Original magnification, ×600; scale bar, 10 μm. Data are from one representative of nine independent experiments with seven healthy controls and nine patients with XLA (**a**), are representative of nine experiments (**b**), are from nine independent experiments (**c**), are pooled from seven independent experiments (**d**) or are representative of four independent experiments (**e**; mean and s.d. in **b**–**d**).

Activated PTKs and PI(3)K in resting XLA neutrophils

Assembly and activation of the cytosolic components and Rac requires the involvement of kinases such as PTKs, PI(3)K and protein kinase C. We thus explored a potential signaling pathway that would lead to the partial assembly of NADPH oxidase. First, we examined the extent of tyrosine phosphorylation of cellular substrates in Btk-deficient and Btk-sufficient neutrophils before and after stimulation with PMA. Btk-deficient neutrophils showed hyperphosphorylation of protein species in the range of 50–53 kilodaltons (kDa), 72 kDa, 85 kDa and 150 kDa at baseline relative to phosphorylation in neutrophils from healthy controls (**Fig. 5a**). TLR4-mediated stimulation led to more phosphorylation of protein species 38 kDa, 50–53 kDa, 60 kDa, 72 kDa and 85 kDa in size in Btk-deficient neutrophils (**Supplementary Fig. 4a**).

In contrast, the baseline PTK activity in monocytes from patients with XLA was unaltered or slightly diminished relative to that of monocytes from healthy controls. TLR2-stimulated activation of PTKs was largely similar or slightly less in the absence of Btk (**Supplementary Fig. 4b**). We were able to directly ascribe the enhanced PTK activity to the absence of Btk, as transduction of recombinant Btk into neutrophils from patients with XLA restored baseline phosphorylation to that seen in neutrophils from healthy controls (**Fig. 5b**).

We next searched for tyrosine-phosphorylated proteins in Btk-deficient neutrophils through the use of phosphorylation-specific antibodies. The expression and activation of Tec and Bmx, TFKs present in neutrophils, was not upregulated in neutrophils from patients with XLA (**Fig. 5c**), which indicated that they did not compensate for Btk function. However, we found that the tyrosine-phosphorylated proteins 50–53 kDa, 72 kDa, 85 kDa and 150 kDa in size were the kinases Lyn and c-Src, Syk, the p85 subunit of PI(3)K (class IA) and FAK, respectively (**Fig. 5d,e**). We found that c-Src, Syk, PI(3)K-p85 and FAK were phosphorylated at their tyrosine residues that have a positive regulatory function. Notably, Lyn, a kinase known to have positive as well as negative roles in the modulation of myeloid function, was phosphorylated at Tyr507, a negative regulatory site[29–31].

We first focused on PI(3)K, as PI(3)K activation targets Rac2 to flavocytochrome b_{558}; this process is important for converting

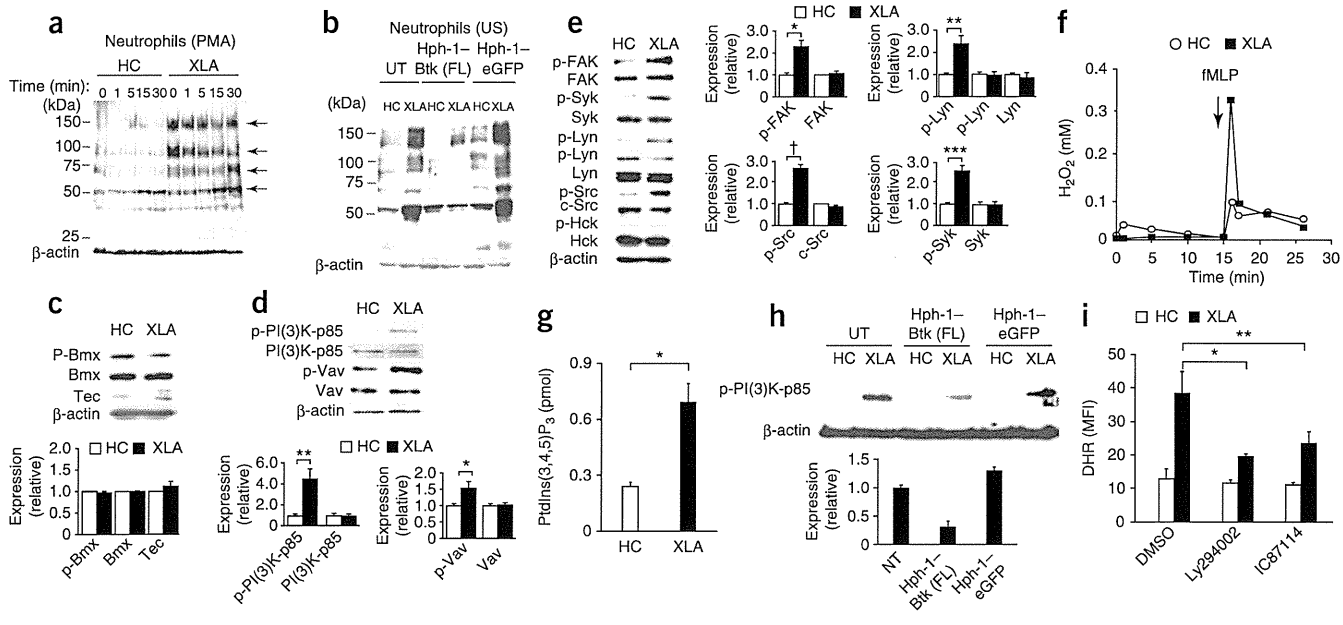

Figure 5 Btk-deficient neutrophils have higher baseline activity of PTKs and PI(3)K, which is reversed by transduction of recombinant Btk protein. (**a**) Immunoblot analysis of phosphorylated tyrosine in lysates of PMA-stimulated neutrophils from healthy controls ($n = 5$) and patients with XLA ($n = 7$). Arrows indicate hyperphosphorylated proteins in neutrophils from patients with XLA at 0 min. (**b**) Immunoblot analysis of phosphorylated tyrosine (as in **a**) in lysates from unstimulated (US) neutrophils from healthy controls ($n = 4$) and patients with XLA ($n = 5$), left untransduced or transduced with Hph-1-tagged full-length Btk or eGFP. (**c,d**) Immunoblot analysis (top) of whole-cell lysates of neutrophils from healthy controls ($n = 5$) and patients with XLA ($n = 7$), probed for total and phosphorylated Bmx and total Tec (**c**) or total and phosphorylated PI(3)K-p85 and Vav (phosphorylated at Tyr508 (PI(3)K-p85) or Tyr174 (Vav); **d**). Phosphorylated Tec was not detected by immunoblot analysis of phosphorylated tyrosine in samples immunoprecipitated with anti-Tec (data not shown). Bottom, quantification of the expression at top, presented relative to expression of β-actin in neutrophils from healthy controls, set as 1. $*P = 0.038$ and $**P = 0.0001$ (Student's *t*-test). (**e**) Immunoblot analysis (left) of neutrophils from healthy controls ($n = 5$) and patients with XLA ($n = 7$), probed for total PTKs and PTKs phosphorylated at Tyr576 and Tyr577 (FAK); Tyr524 and Tyr525 (Syk); Tyr507 (Lyn; top) or Tyr397 (Lyn; bottom); (Tyr416 (c-Src); and Tyr411 (the kinase Hck). Phosphorylated PTKs Fgr and Yes were undetectable (data not shown). Right, quantification as in **c,d**. $*P = 0.033$, $**P = 0.004$, $***P = 0.0007$ and $\dagger P = 0.0002$ (Student's *t*-test). (**f**) H_2O_2 production by fMLP-stimulated neutrophils from healthy controls and patients with XLA ($n = 5$ per group). (**g**) Enzyme-linked immunosorbent assay of phosphatidylinositol-(3,4,5)-trisphosphate (PtdIns(3,4,5)P_3) in unstimulated neutrophils from patients with XLA ($n = 5$). $*P = 0.0005$ (Student's *t*-test). (**h**) Immunoblot analysis (top) of phosphorylated PI(3)K-p85 in neutrophils from healthy controls and patients with XLA ($n = 5$ per group), left untransduced or transduced with Hph-1–tagged full-length Btk or eGFP. Detection of phosphorylated PI(3)K-p85 in neutrophils from healthy controls required longer exposure. Below, quantification of results above, presented relative to the expression of phosphorylated PI(3)K-p85 relative to that of β-actin in neutrophils from patients with XLA, set as 1. (**i**) Production of ROS in neutrophils from patients with XLA, treated with dimethyl sulfoxide (DMSO) or preincubated with Ly294002 (universal PI(3)K inhibitor; 50 μM)[32] or IC87114 (PI(3)Kδ inhibitor; 1 μM (a concentration that does not inhibit PI(3)Kα, PI(3)Kβ or PI(3)Kγ)[33]) and stimulated with fMLP. $*P = 0.006$ and $**P = 0.003$ (Student's *t*-test). Data are representative of or pooled from six (**a,f**), seven (**b–e**), four (**g**), eight (**h**) or five (**i**) independent experiments (mean and s.d. in **c–e,g–i**).

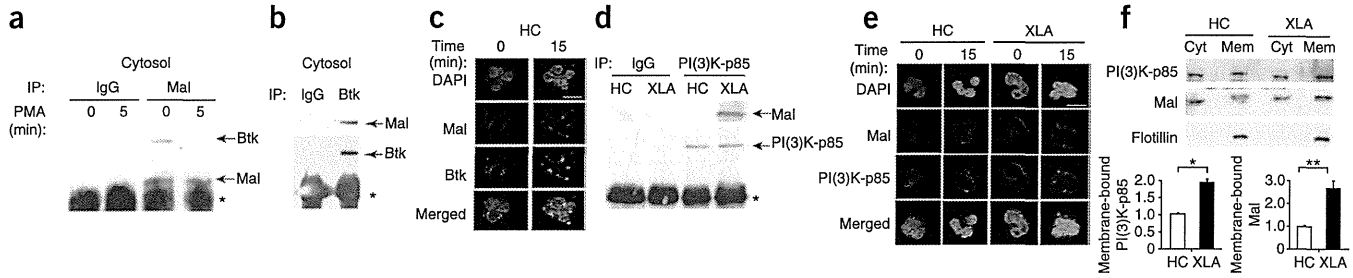

Figure 6 Mal in neutrophils from healthy controls associates with Btk in the resting state and translocates to the plasma membrane after stimulation, whereas Mal associates with PI(3)K at the plasma membrane in Btk-deficient neutrophils. (**a**,**b**) Coimmunoprecipitation analysis of Btk and Mal in the cytoplasmic fraction of neutrophils from healthy controls, left unstimulated (0 (**a**), **b**) or stimulated for 5 min with PMA (5 (**a**)). IP, immunoprecipitation; IgG, control antibody. *, immunoglobulin light chain (**a**) or heavy chain (**b**). (**c**) Confocal microscopy of neutrophils from healthy controls, left unstimulated (0) or stimulated for 15 min with PMA (15), then stained with anti-Mal (red) and anti-Btk (green) and counterstained with DAPI. Original magnification, ×600; scale bar, 10 μm. (**d**) Coprecipitation analysis of PI(3)K-p85 and Mal in membrane fraction of neutrophils from healthy controls and patients with XLA. *, immunoglobulin heavy chain. (**e**) Confocal microscopy of neutrophils from healthy controls and patients with XLA, left unstimulated or stimulated for 15 min with PMA, then stained with anti-Mal (red) and anti-PI(3)K-p85 (green) and counterstained with DAPI. Scale bar, 10 μm. (**f**) Immunoblot analysis (above) of PI(3)K-p85 and Mal in the cytoplasm and plasma membrane of unstimulated neutrophils from healthy controls and patients with XLA. Below, quantification of results above, presented relative to the expression of flotillin in neutrophils from healthy controls, set as 1. $*P = 0.0035$ and $**P = 0.0021$ (Student's *t*-test). Data are representative of three (**a**,**b**), four (**c**,**e**), six (**d**) or seven (**f**) independent experiments (mean and s.d. in **f**).

neutrophils into a 'primed' state in which they are ready for complete activation of NADPH oxidase triggered by stimuli such as fMLP. Indeed, Btk-deficient neutrophils were in a primed state, as fMLP alone elicited excessive production of ROS (**Fig. 5f**). Greater phosphorylation of PI(3)K-p85 was accompanied by more enzymatic activity, as shown by more baseline production of phosphatidylinositol-(3,4,5)-trisphosphate and by phosphorylation of the adaptor Vav (**Fig. 5d**,**g**). Furthermore, augmented PI(3)K activation was normalized, although only partially, by transduction of full-length Btk linked to Hph-1 (**Fig. 5h**).

The importance of PI(3)K in inducing the primed state was supported by data showing inhibition of fMLP-driven production of ROS by preincubation of Btk-deficient neutrophils with the universal PI(3)K inhibitor LY294002 at a concentration of 50 μM (refs. 32,33). We observed this inhibition in cells incubated with the PI(3)Kδ–specific inhibitor IC87114 at a concentration of 1 μM (ref. 33) but not in those incubated with the PI(3)Kγ–specific inhibitor AS605240 at a concentration of 8 nM (ref. 34; **Fig. 5i** and **Supplementary Fig. 5a**). These findings suggested PI(3)Kδ activation was involved in the excessive ROS response.

Interaction of membrane-targeted Mal with PI(3)K

We next sought the reason for the PI(3)K activation in the absence of Btk. For this, we first focused on a molecule that interacts with both Btk and PI(3)K. Evidence obtained with monocytes indicates that Mal is a critical component of TLR2-TLR4 signaling and is a target of Btk[13,14,20,21]. The TLR signal triggers activation of Btk, which in turn phosphorylates Mal. Phosphorylated Mal translocates to the plasma membrane via phosphatidylinositol-(4,5)-bisphosphate ($PtdIns(4,5)P_2$) and then interacts with and activates PI(3)K[35].

Unexpectedly, coimmunoprecipitation assays of neutrophils from human controls demonstrated that Mal was associated with Btk in the resting state (**Fig. 6a**,**b**). We observed colocalization of Mal and Btk in the cytoplasm and, after activation of cells with PMA, we detected the Mal-Btk complex at the membrane by immunofluorescence staining (**Fig. 6c**).

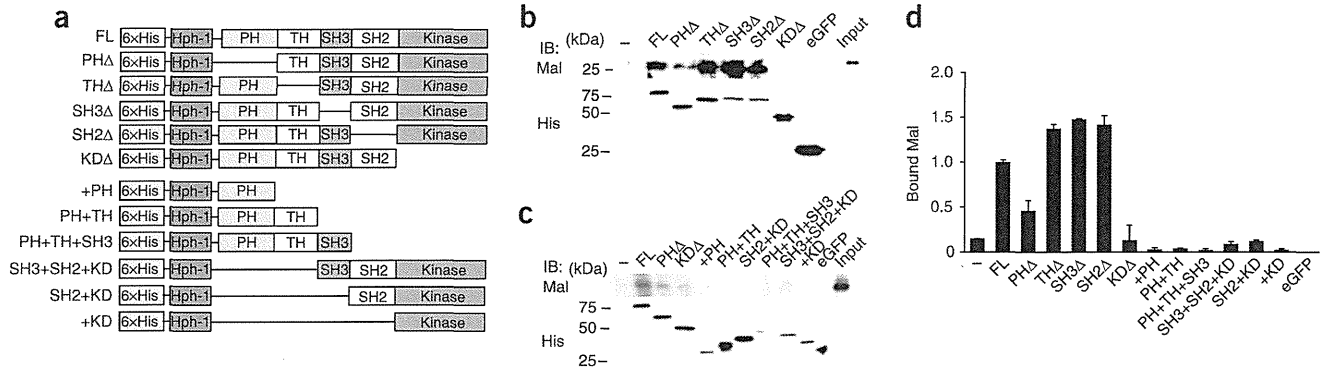

Figure 7 Btk associates with Mal at the PH and kinase domains. (**a**) Hph-1–tagged Btk constructs: full-length Btk (FL); Btk mutants with deletion of the PH domain (PHΔ), Tec homology (THΔ), SH3 domain (SH3Δ), SH2 domain (SH2Δ) or kinase domain (KDΔ); and Btk mutants with truncation retaining (+) only some domains (bottom six). (**b**,**c**) Immunoblot analysis (IB) of Mal (top) in extracts of cytoplasm of neutrophils from healthy controls, incubated with nickel beads bound to Hph-1–tagged recombinant full-length Btk or the deletion mutants (**b**) or truncation mutants (**c**) in **a**, or to Hph-1–tagged eGFP (negative control). Below, immunoblot analysis after rebinding to nickel beads, probed with anti-histidine (His). To make these as equimolar as possible, more beads were added for the +PH, PH+TH+SH3, SH3+SH2+KD and +KD constructs. Input, cytoplasmic extracts without precipitation. (**d**) Quantification of Mal bound to the recombinant Btk proteins based on the results in **b**,**c** ($n = 4$ donors), presented to results for full-length Btk, set as 1. Data are representative of four experiments (**b**,**c**) or are a summary of four independent experiments (**d**; mean and s.d.).